

**INVESTIGATING THE CONCEPT OF FRAUNHOFER LINES AS A POTENTIAL  
METHOD TO DETECT CORONA IN THE WAVELENGTH REGION 338nm – 405nm  
DURING THE DAY**

School of Electrical and Information Engineering

University of the Witwatersrand

N.Maistry

Copyright ©

School of Electrical and Information Engineering

University of the Witwatersrand, Johannesburg

Revision 10

12 February 2015

## ABSTRACT

It is essential to detect corona discharge as a symptom of insulation breakdown in high voltage applications. However the accuracy of such a measurement is often reduced due to the existence of solar background noise in the signal. Fraunhofer lines in the solar spectrum are areas of the solar spectrum where the solar radiation is lower in intensity due to certain wavelengths of light being absorbed by gases in the sun. Analysing the corona and solar spectra reveals that there exists an overlap at certain wavelengths between corona peaks and Fraunhofer lines specifically between the 300nm - 400 nm wavelength range. This thesis will explore the potential of evaluating corona activity at these Fraunhofer lines and through signal processing optimise the signal to noise ratio. One of the signal processing techniques used was the implementation of an optical band-pass filter. From the results obtained it was determined that the purchased optical filter was not filtering out the solar radiation and hence no corona was detected. The signal to noise ratio was 0.0314. Consequently it was decided that the optical filter specifications (i.e. (FWHM) and central wavelength (CWL)) were not ideal. Hence a new approach of simulating an optical narrow band-pass filter in MATLAB was applied. The MATLAB model allowed the filter to adjust its bandwidth along the wavelength range until the highest signal to noise ratio was obtained. The signal to noise ratio was 2.121. The simulated filter specifications that generated the highest signal to noise ratio had a FWHM of 0.05nm and CWL of 357.558nm which coincided with the wavelength of a different Fraunhofer line and a different corona peak. The results verified that with the newly designed filter the signal to noise ratio increased by 67%. Thereafter cross correlation was performed for extracting the corona signal from the solar background noise. Correlation proved to be an efficient technique to detect corona in the presence of solar radiation. In essence Fraunhofer lines can be used to detect corona activity during the daytime with the implementation of a suitable filter as well as through cross correlation.

## **ACKNOWLEDGEMENT**

*I would never have been able to finish my dissertation without the guidance of Council of Scientific Research (CSIR), University of Witwatersrand, help from friends and support from my family.*

*I would like to express my deepest gratitude to Robert Schutz for his excellent guidance, caring nature, patience, and for providing me with an excellent atmosphere for doing research. Robert was always there cheering me up and stood by me through the good times and bad. I would like to thank Roel Stolper and Peet De Wet, who as good mentors were always willing to help and give their best suggestions. To John Van Coller for giving ideas for the improvement of the study; financial support and for his patience, understanding and encouragement. I would also like to thank my mother, sisters, and brothers. They were always supporting me and reassuring me with their best wishes.*

*Finally I will like to thank God my Saviour, for giving me the wisdom, strength, support and knowledge to conduct the research and for giving me the determination and guidance to pursue my studies and surpass all the trials I encountered to make this research possible.*

***This is for you ma and thatha!!!***

## PREFACE

This thesis is submitted to the School of Electrical and Information Engineering at the University of Witwatersrand Johannesburg in fulfilment of the requirements for an MSc degree in Electrical Engineering. The research has been carried out between 1.04.2013 and 1.10.2014 at the Council of Scientific Research (CSIR) Pretoria, Department of Sensor Science and Technology, by which I was hired as an MSc student for the entire project period. The project has been followed full time by two Supervisors: Dr John van Coller (Department of Electrical Engineering, Witwatersrand) and Robert Schutz (CSIR).

The School of Electrical and Information Engineering at the University of Witwatersrand and Council of Scientific Research has funded the research leading to this thesis: **Investigating the concept of Fraunhofer lines as a potential method to detect corona in the wavelength region 338.67nm – 405nm during the day.**

The funding has been vital for this research project. Travelling to conferences, visits at research institutions, renting of laboratory equipment and performance and field measurements were made possible thanks to support from these institutions.

The conception of the thesis was to look at a new innovative method of detecting corona outside the solar blind region during the day. The effect of solar radiation is a fundamental factor to consider when detecting corona. The corona emission in the 280nm – 405nm spectral range cannot be detected during daytime due to the extremely disturbing background of solar radiation. Closer study of the solar spectrum showed a large number of narrow dark lines i.e Fraunhofer lines. These lines represent wavelengths of light that have been removed by gases present in the outer layers of the sun. The effect of this is that there are a few windows at well-defined locations in the electromagnetic spectrum. The topic was thus established that if it was possible to exploit the concept of Fraunhofer lines as a potential method to detect corona during the day then through effective signal processing the signal to noise ratio i.e. the corona signal to solar background noise could effectively be improved.

*I cannot express the long days spent in the lab, battling shoulder to shoulder with my fellow scientists and friends, the hope for good results and the sadness and tiredness with each failed attempt.*

The only way I can express my journey is through the following quote by Calvin Coolidge:

***“Nothing in the world can take the place of persistence. Talent will not; nothing is more common than unsuccessful men with talent. Genius will not; unrewarded genius is almost a proverb. Education will not; the world is full of educated derelicts. Persistence and determination alone are omnipotent. The slogan, ‘press on’ has solved, and always will solve, the problems of the human race”***

*Nattele Maistry*

# CONTENTS

<b>LIST OF FIGURES.....</b>	<b>1</b>
<b>LIST OF GRAPHS.....</b>	<b>2</b>
<b>LIST OF TABLES.....</b>	<b>3</b>
<b>LIST OF SYMBOLS AND ABBREVIATIONS.....</b>	<b>3</b>
<b>CHAPTER1: INTRODUCTION .....</b>	<b>6</b>
1.1 Overview .....	6
1.2 Statement of Problem .....	6
1.3 Possible solution to the corona detection problem .....	7
1.4 Research Questions .....	8
1.5 The Importance of the Research Questions .....	8
1.6 Scope of Study.....	8
1.7 Organisation of the report.....	9
<b>CHAPTER 2: LITERATURE SURVEY .....</b>	<b>10</b>
2.1 Corona .....	10
2.1.1 Basic ionisation processes.....	10
2.1.2 Electron emission from conductor surfaces .....	11
2.1.3 Electron avalanching.....	11
2.1.4 Discharges in a non-uniform electric field .....	13
2.1.5 Discharges in a uniform electric field .....	13
2.1.6 Current versus voltage characteristics of discharges .....	14
2.1.7 Types of corona and their spectra.....	16
2.1.8 Parameters of corona .....	19
2.1.9 Effects of corona .....	24
2.1.10 Methods to reduce corona .....	24
2.1.11 Presently used corona detection methods.....	25

2.2 Fraunhofer lines .....	26
2.2.1 The Fraunhofer lines .....	27
2.2.2 Measurement of the Fraunhofer lines .....	30
2.2.3 Overlap between the Fraunhofer lines and the corona emission peaks .....	30
2.3 Signal Processing .....	31
2.3.1 Signal-to-noise ratio (SNR) .....	31
2.3.2 Filters .....	32
<b>CHAPTER 3: METHODOLOGY .....</b>	<b>35</b>
<b>CHAPTER 4: EQUIPMENT USED AND EXPERIMENTAL RESULTS .....</b>	<b>36</b>
4.1 Equipment used .....	36
4.2 Experimental and Signal Processing Results .....	40
<b>CHAPTER 5: CONCLUSIONS AND RECOMMENDATIONS FOR FURTHER WORK .....</b>	<b>54</b>
5.1 Conclusions .....	54
5.2 Recommendations for further work .....	55
<b>REFERENCES .....</b>	<b>56</b>
<b>APPENDIX .....</b>	<b>58</b>
Matlab code .....	58

## LIST OF FIGURES

Figure 1: Absorption of solar radiation by the earth's atmosphere (Averill, 2007).....	6
Figure 2: Visible solar light spectrum (Maruvada, 2011).....	7
Figure 3: Solar spectrum (Bird, et al., 1983).....	7
Figure 4: Spectrum showing absorption lines (Averill & Eldredge, 2007).....	8
Figure 5: Electron avalanche (Loeb, 1965).....	12
Figure 6: Gas discharge in a uniform electric field arrangement.....	13
Figure 7: Voltage versus current characteristic of the discharge (Maruvada, 2011).....	14
Figure 8 : Voltage versus current characteristic for a gas discharge (Bouchacourt, et al., 2003).....	15
Figure 9: DC corona light spectrum (Maruvada, 2000).....	16
Figure 10: AC corona spectrum (Chen, 1998).....	17
Figure 11: DC corona spectra showing increased intensity and longer spectral wavelength (Shixiu, 1998).....	18
Figure 12: Spectra visible beyond 730 nm.....	18
Figure 13: Corona emission in air (Shimizu, 2011).....	19
Figure 14: Effect of conductor surface temperature and conductor radius.....	20
Figure 15: Effect of altitude and conductor radius on the corona onset gradient (Maruvada, 2011).....	20
Figure 16: Corona onset gradients of hardware electrodes (Maruvada, 2011).....	21
Figure 17: Corona inception voltage for rod-plane versus gap length with various rod radii, r (Javadi, et al., 2010)...	22
Figure 18: Gap voltage and corona current wave shape for a rod plane gap ( $r=2.48\text{mm}$ and $d=4\text{cm}$ ).....	22
Figure 19: Radiation spectrum (Vosloo, et al., 1997).....	25
Figure 20: Solar spectrum generated in SMARTS (Bird, et al., 1983).....	26
Figure 21: Spectrum showing absorption lines (Averill, 2007).....	27
Figure 22: Solar spectra in the ultra-violet region demonstrating the major broad-band Fraunhofer lines (Kingsley, 1990).....	27
Figure 23: Diagram of a simple spectroscope (Averill, 2007).....	30
Figure 24: Corona spectrum (Schulze, et al., 2010).....	31
Figure 25: Absorption filter (Murphy, et al., 1999).....	32

Figure 26: Anatomy of an interference filter (Murphy, et al., 1999) .....	32
Figure 27: Green interference filter (Murphy, et al., 1999) .....	33
Figure 28: Band-pass filter transmission (Govire & Pete, 2007).....	34
Figure 29: Relationship between fibre diameter and resolution (Wako, 2011) .....	37
Figure 30: Schematic describing operation of the cosine corrector .....	38
Figure 31: Cosine corrector (Jorgie, 2013).....	38
Figure 32: Point-sphere corona source .....	39
Figure 33: Converging Lens .....	39
Figure 34: Cassegrain (SC, 2001).....	39
Figure 35: Hipotronics power supply .....	40
Figure 36: Experimental setup.....	41
Figure 37: Schematic of lens alignment process .....	43
Figure 38: Application of lens alignment setup.....	43
Figure 39: Experimental setup.....	44
Figure 40: Schematic of experimental setup.....	45
Figure 41: Photograph of experimental setup.....	46
Figure 42: Experimental Setup .....	47
Figure 43: Experimental setup.....	49
Figure 44: Photograph of Experimental setup .....	49
Figure 45: Experimental setup.....	51

## LIST OF GRAPHS

Graph 1: Solar spectrum recorded and solar spectrum from SMARTSs	40
Graph 2: Solar spectrum with and without cosine corrector	41
Graph 3: Calculated cosine corrector transmission curve	42
Graph 4: Solar spectrum indicating Ca II at 393.3682nm(blue line in graph)	42
Graph 5: Recorded corona spectra at varying DC Voltage	46



Graph 6: Recorded positive and negative corona spectra	48
Graph 7: Measured absorption and transmission of the optical filter	49
Graph 8: Specified transmission and absorption of the optical band-pass filter	50
Graph 9: MATLAB generated transmission curve of the filter and corona and solar spectra	51
Graph 10: Ideal filter transmission	52
Graph 11: Corona and solar spectra	53

## LIST OF TABLES

Table 1: The Dominant Solar Fraunhofer lines (Bird, et al., 1983).....	28
Table 2: Major Fraunhofer lines.....	30
Table 3: Overlap of corona and solar spectra at the Fraunhofer lines.....	31
Table 4: Slit width vs optical resolution.....	36
Table 5: Specifications of the optical band-pass filter.....	37
Table 6: Calculated and measured voltages.....	44
Table 7: Results.....	52
Table 8: Correlation results.....	52

## LIST OF SYMBOLS AND ABBREVIATIONS

### Symbols

$\delta$	Air density correction factor
R	Correlation
N	Density of gas, in $m^{-3}$
$V_D$	Disruptive critical voltage, in V
d	Distance between surfaces, in cm

$v$	Drift velocity, in m/s
$E$	Electric field, in V/m
$\mu$	Electron mobility, in $m^2/V\text{-sec}$
$M$	Electron multiplication
$I_0$	Incident light intensity, in lux
$\alpha$	Ionisation coefficient
$N_e$	Number of electrons
$\%T_\lambda$	Percent transmission at a particular wavelength
$E_0$	Empirical constant depending on nature of the applied voltage in kV/cm
$K$	Empirical constant depending on nature of the applied voltage
$E_c$	Corona onset gradient , in kV/cm
$P_{\text{noise}}$	Power of noise, in watts
$P_{\text{signal}}$	Power of signal, in watts
$r$	Radius of wire/conductor, in cm
$I$	Transmitted light intensity, in lux
$m$	Surface irregularity factor
$V_v$	Visual critical voltage, in V
$\lambda$	Wavelength, in nm
$U_0$	Saturation Voltage

## Abbreviations

CWL	Central wavelength
HV	High voltage
OD	Optical density
SNR	Signal-to-noise ratio
SMARTS	Simple Model of the Atmospheric Radiative Transfer of Sunshine
FWHM	Full width half maximum
RIV	Radio interference voltage
AC	Alternating current
DC	Direct current
HF	High Frequency
UV	Ultra-violet
IR	Infrared
EMI	Electromagnetic interference
EM	Electromagnetic

# CHAPTER1: INTRODUCTION

## 1.1 Overview

A corona discharge is a glowing partial discharge from conductors and insulators due to excitation of the air molecules, when the local electrical field exceeds a critical value. The excitation of the air molecules leads to the emission of UV radiation. Consequently a problem or defect on a component creating a local high electric field will produce corona activity. The early detection of corona is fundamental in preventing transmission line failures.

The corona discharge emits radiation in the 240 nm – 440 nm spectral range, mostly in the UV range and is therefore invisible to the human eye, though relatively weak emissions at around 400 nm might be observed at night under conditions of absolute darkness. Corona emission in the 280 nm – 405 nm spectral range cannot be detected during daytime due to the extremely disturbing solar radiation background (Loeb, 1939).

UV cameras to detect corona in daytime are increasingly being used for periodic inspections. These cameras can provide information on the exact location of corona. Detection of corona using UV cameras currently is in the 240 nm – 280 nm solar blind UV range (Vosloo, et al., 1997). In the solar blind region, due to the ozone layer in the stratosphere, solar radiation is completely blocked and the background solar radiation at the earth's surface is zero. This absence of background solar radiation can be utilized to detect corona at extremely weak levels of UV emittance.

## 1.2 Statement of Problem

Figure 1 shows the amount of absorption at different wavelengths by the atmosphere. It is presented in terms of the half-absorption altitude, which is the altitude (measured from the earth's surface) where half of the radiation at a given wavelength incident on the upper atmosphere has been absorbed.

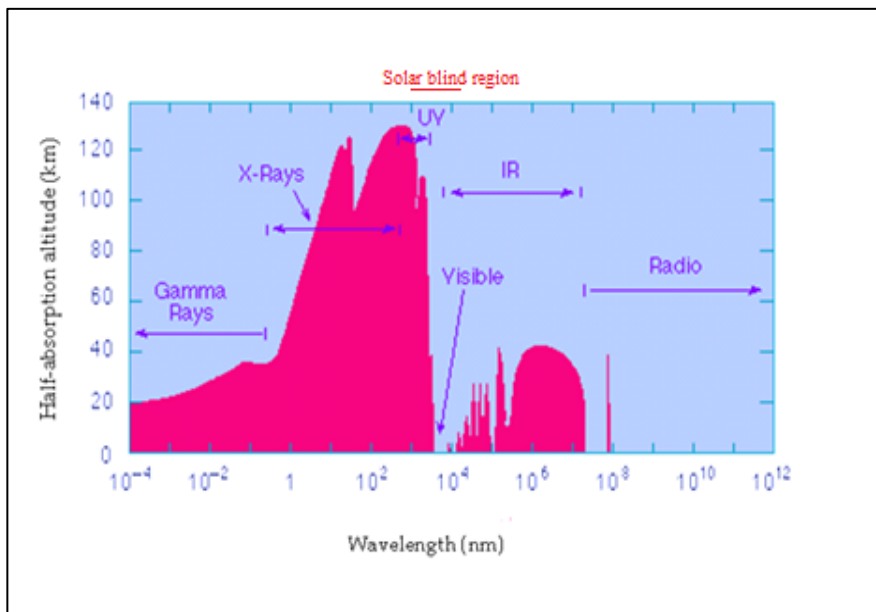


Figure 1: Absorption of solar radiation by the earth's atmosphere (Averill, 2007)

Detection of corona in daylight is feasible by utilizing the solar blind region and a solar blind filter (the blue graph in Figure 2).

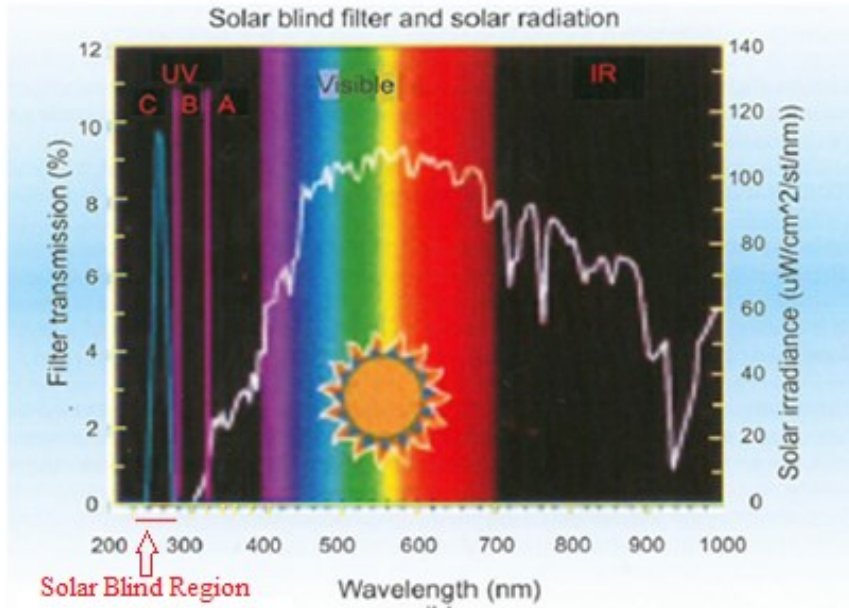


Figure 2: Visible solar light spectrum (Maruvada, 2011)

Detection limited to this band has the advantage of a much better SNR however the corona emittance in the solar blind region is very weak thus an image intensifier (which is extremely expensive) is required to amplify and convert low amplitude signals into visible quantities. The CoroCam and DayCor are examples of video cameras for viewing corona emittance in the solar blind region. However outside the solar blind region specifically between 300nm - 400nm many corona peaks which are of a considerably higher intensity exist. Amplification is not required and consequently no need for an image intensifier. (Vosloo, et al., 1997).

### 1.3 Possible solution to the corona detection problem

Solar radiation is a fundamental factor to consider when detecting corona. It is therefore important to understand the solar spectrum. Figure 3 is a standard spectrum of solar radiation.

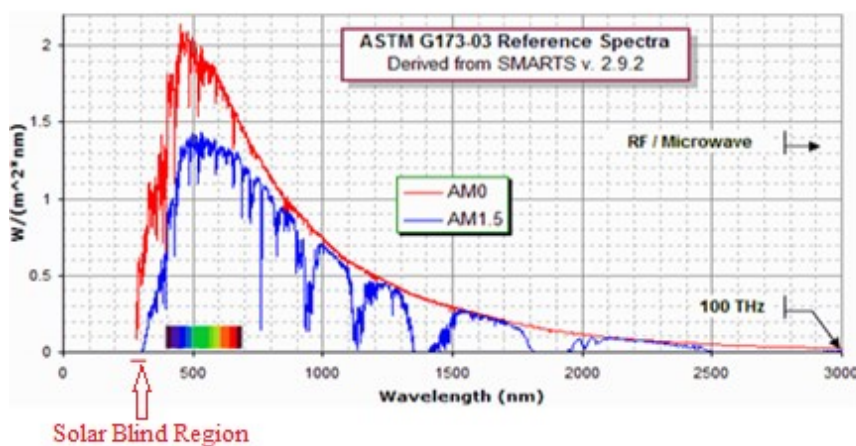


Figure 3: Solar spectrum (Bird, et al., 1983)

Analysing the solar spectrum shows that the solar spectrum is interrupted by a large number of narrow dark lines as shown in Figure 4.

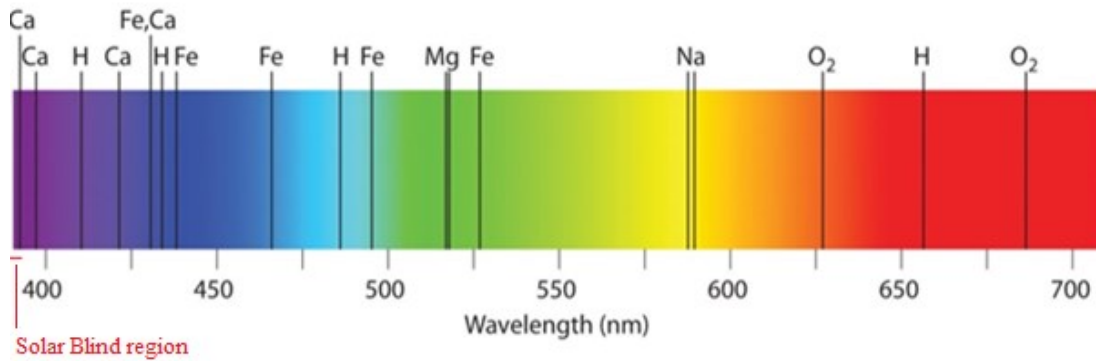


Figure 4: Spectrum showing absorption lines (Averill & Eldredge, 2007)

These lines are known as Fraunhofer lines. These lines represent the wavelengths of light that have been removed by gases present in the outer layers of the sun (Walloston, 1802). The effect of this is that there are a few regions of solar radiation darkness at well-defined locations in the electromagnetic spectrum.

The question is whether it is possible to exploit the Fraunhofer lines as a potential method to detect corona in the wavelength range 338.67 nm – 405 nm during the day.

#### 1.4 Research Questions

The following research questions will be addressed in the thesis:

1. Is there a correlation between measured and published corona spectra and solar spectra?
2. Do the wavelength and intensity of the corona peaks vary with applied voltage?
3. Can signal processing improve the SNR i.e. the level of the corona signal relative to the level of solar background noise?
4. Can these discontinuities in the solar spectrum be a potential method of detecting corona within the wavelength range 338.67 nm – 405 nm during the day?

#### 1.5 The Importance of the Research Questions

It was important to verify solar and corona spectra with existing published spectra as well as to obtain actual corona spectra. Furthermore it was significant to determine whether an overlap existed between Fraunhofer lines and the corona peaks. Once verification of the overlap was established it was central to investigate whether signal processing techniques could be applied to the corona and Fraunhofer spectra to improve the SNR with the potential outcome of developing a cheaper corona detecting camera.

#### 1.6 Scope of Study

All the corona generation experiments used a point-sphere corona source. All the experiments were conducted at the CSIR, Pretoria. A Starline AvaSpec 2048L spectroradiometer was used for measuring the spectra. An optical band-pass filter was provided by Materion. The wavelength range was chosen to achieve high resolution and to ensure that a corona peak and a Fraunhofer line overlapped.

## 1.7 Organisation of the report

The report has been divided into five chapters.

**Chapter 1 Introduction:** This chapter deals with the rationale, objectives and scope of the study.

**Chapter 2 Literature Survey:** This chapter provides the necessary background information which will facilitate the understanding of the thesis. Furthermore existing literature on corona, Fraunhofer lines and signal processing will be presented.

**Chapter 3 Methodology:** The approach of the study will be described in this chapter .

**Chapter 4 Experimental Equipment and Experimental Results :** The materials used and adopted for the study are described in this chapter together with the experimental and signal processing results. In addition an analysis of the results will be presented .

**Chapter 5 Conclusions and Recommendations for future work:** This chapter concludes the study and provides recommendations for further work.

## CHAPTER 2: LITERATURE SURVEY

### 2.1 Corona

Corona occurs when the electric fields adjacent to the conductors of HV transmission lines are high enough to cause excitation of the adjacent air molecules. Corona is associated with a faint glow around the conductor, a hissing sound and the production of ozone (Maruvada, 2011).

The following section will describe the physics of corona discharges and the published spectra of corona. Furthermore the parameters of corona will be outlined as well as the various types of corona. The effects of corona as well as the methods to reduce corona will be described. Finally the existing corona detection methods will be discussed.

#### 2.1.1 Basic ionisation processes

Air is the most important insulating medium on HV transmission lines. The main constituents of air are the following:

- Nitrogen - 78.09%
- Oxygen – 20.95%
- Argon – 0.93%
- Traces of Carbon Dioxide, Neon, Helium, Krypton etc,

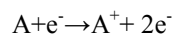
The volume percentage of water vapour depends on ambient temperature and is highest near the equator and decreases towards the poles. However the volume percentage of gaseous constituents is relatively constant (Maruvada, 2011). Under normal conditions the gases and water molecules in air are electrically neutral. However naturally occurring phenomena, e.g. gamma rays produced by radioactive processes or cosmic radiation, generate enough energy to ionise the gas molecules giving rise to positive ions and free electrons which prevent the air from being electrically neutral. The presence of even a low concentration of charged particles makes air conducting. In addition air is susceptible, under high electric fields, to electrical discharge phenomena such as breakdown and corona (Maruvada, 2011).

The following symbols are used to describe the ionisation processes:

- A is a neutral atom or molecule.
- $e^-$  is a free electron.
- $A^+$  is a positive ion and  $A^-$  is a negative ion.
- $A^*$  is an atom or molecule in an excited state.
- $eV_i$  is the energy required to ionize a neutral atom or molecule.
- $A^m$  is a metastable

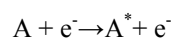
##### 2.1.1.1 Ionisation by collision

Ionisation by collision is a process where a free electron transfers its kinetic energy to a neutral atom or molecule releasing another free electron (Maruvada, 2011).

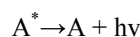


##### 2.1.1.2 Photo-ionisation and photo-emission

If the collision with any electron is not able to ionise the molecule, the result of the collision could be an excited molecule (Maruvada, 2011).

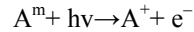
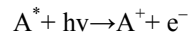
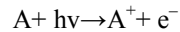


Since the excited state is not permanent, the excited atom will return to its neutral state emitting a photon with energy  $h\nu$  (Maruvada, 2011).



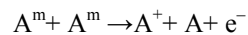
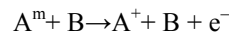


The energy emitted as a photon is then absorbed by a neutral atom. In the case of having enough energy to ionise, different reactions can take place. Some of them are (Maruvada, 2011):



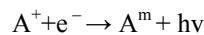
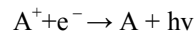
#### 2.1.1.3 Ionisation by collision with meta-stables

Ionization by collision with meta-stables takes place when an atom in a meta-stable state collides with another atom. As a result, a positive ion and a free electron are created (Maruvada, 2011).



#### 2.1.1.4 De-ionisation by recombination

Deionization by recombination is where a free electron becomes attached to a positive ion causing the atom or molecule to return to its neutral state, and releasing energy in the form of a photon (Maruvada, 2011).



#### 2.1.2 Electron emission from conductor surfaces

Electron emission from conductor surfaces is an important factor in gas discharges, particularly corona. The electrons at the peripheral layer of atoms on the metal surface are free to move within the metal. If the electron gains sufficient energy, known as the work function, it can escape from the metal surface (Maruvada, 2011). Electrons may be emitted due to the impact of positive ions on metal surfaces. The number of electrons emitted increases with the energy of the impinging positive ions. To have net electron emission from the surface each ion must extract two electrons, one of which is necessary to neutralise the ion. In gas discharges the high energy photons impinging on the conductor surface may also be a cause of electron emission (Maruvada, 2011).

#### 2.1.3 Electron avalanching

The building block of all dc and ac coronas, as of most other gas discharges is the Townsend electron avalanche. The basic mechanism involved in the corona discharge occurs as a series of steps as shown in Figure 5.

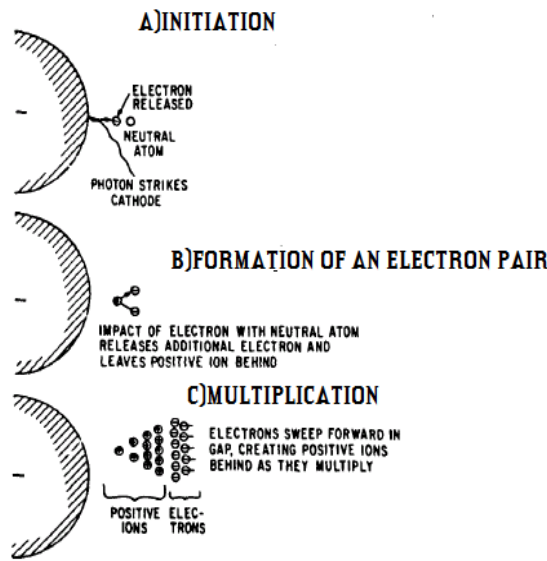


Figure 5: Electron avalanche (Loeb, 1965)

When a voltage is applied to the test electrode geometry, the free electrons are accelerated. Some of these electrons acquire enough energy so that when they collide with atoms, more electrons are released. Many of the collisions that take place are elastic i.e. the electron loses very little of its kinetic energy. When an electron has sufficient energy to strike an atom and cause excitation, the atom jumps to a higher energy state and when it returns to its neutral state, it emits energy in the form of light (visible corona). The 'avalanche' produces positive and negative ions (Loeb, 1965).

### 2.1.3.1 Mechanism of an electron avalanche

Townsend developed a coefficient to describe the number of electrons that are produced from a single electron traveling in a uniform electric field (Goldman & Sigmond, 1982).

$$dN_e(r) = N_e(r) (\alpha - n) dr = N_e(r) \alpha' dr \quad (1)$$

Or

$$N_e(r) = N_e(0) \exp \int_0^r \alpha' dx \quad (2)$$

-where

- $\alpha$  is the primary ionisation coefficient.
- $n$  is the attachment coefficient
- $\alpha' = \alpha - n$  is the effective ionisation coefficient
- $\mu$  is the mobility of the electron

To get a self-sustained discharge, feedback is necessary, and so secondary ionization is required (Goldman & Sigmond, 1982). This feedback mechanism can be described by  $\gamma$  processes. The secondary ionization coefficient  $\gamma$  is defined as the number of secondary electrons in the ionization region. The  $\gamma$  processes can be divided into cathode processes and gas processes. From the cathode, the secondary electrons can be liberated due to positive ion impact (positive ion feedback  $\gamma_{ic}$ ), by metastable impact (metastable feedback  $\gamma_{mc}$ ) or by photon irradiation (photon feedback  $\gamma_{pc}$  due to the photo-effect). In the gas, the secondary electrons can be produced due to photon collision  $\gamma_{pg}$ .

The self-sustainment of a discharge can be characterized by a reproduction factor, which is defined as:

$$\mu_r = \gamma \int_0^d \alpha \exp\left(\int_0^r \alpha' dx\right) dr \quad (3)$$

- where

$\gamma$  is the secondary ionization coefficient  $\gamma = \gamma_{ic} + \gamma_{mc} + \gamma_{pg}$

$d$  denotes the length along the electric field.

The Townsend's criterion for a self-sustained discharge is when  $\mu_r=1$

#### 2.1.4 Discharges in a non-uniform electric field

Most air gaps associated with HV transmission lines are characterised by non-uniform electric field distributions. The electric field is non-uniform with the highest electric field occurring at the electrode and decreasing rapidly near the HV electrode and more gradually near the ground surface. As the voltage across the gap is increased, ionisation is initiated at the surface of the HV electrode. At a certain distance from the HV electrode surface the electric field falls to a low level and ionisation stops. The discharge activity is confined to a small region in the vicinity of the HV electrode. The self-sustained discharge is limited to the stressed part of the gap and is known as a partial breakdown or corona discharge. Since the electric field is non-uniform, the ionisation coefficient  $\alpha$  is a function of distance from the HV electrode shown by (Maruvada, 2011):

$$1 - \gamma e^{\int_0^{d_i} \alpha(x) dx} = 0 \quad (4)$$

The integration is to a distance  $d_i$  at which  $\alpha=0$  or ionisation ceases. For gases the ionisation coefficient can be modified to include attachment and the corona onset criterion is (Maruvada, 2011) :

$$1 - \gamma e^{\int_0^{d_i} (\alpha(x) - n(x)) dx} = 0 \quad (5)$$

The limit of integration  $d_i$  corresponds to the boundary where the ionisation coefficient equals the attachment coefficient so that beyond which, no net ionisation can take place (Maruvada, 2011).

#### 2.1.5 Discharges in a uniform electric field

A uniform field gap with positive voltage applied to the anode with the cathode grounded through an ammeter (sensitive to measure small currents) is shown in Figure 6. An electron avalanche created by free initial electrons at the cathode surface is shown by the arrow in Figure 6 .

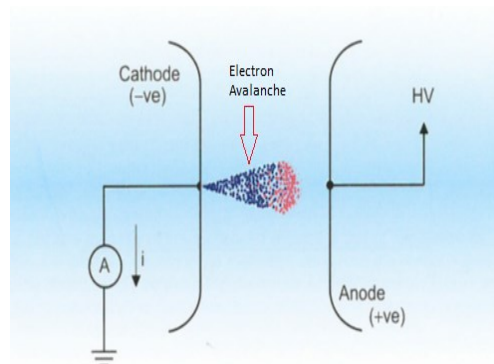


Figure 6: Gas discharge in a uniform electric field arrangement. (Maruvada, 2011)

Free electrons may be produced at the cathode either by natural ionisation processes or by artificial illumination with UV light. These free electrons will be accelerated from the cathode at  $x = 0$  towards the anode at  $x = d$  due to the presence of an electric field. These free electrons will collide with neutral gas molecules and produce additional free electrons. The avalanche eventually crosses the gap.

### 2.1.6 Current versus voltage characteristics of discharges

Discharges are distinguished by their current versus voltage characteristics, the current density and breakdown voltage. These main characteristics depend on the geometry of the electrodes, the gas used and the electrode material. The discharge type changes with the discharge current.

The discharge process for a uniform field gap where a voltage  $U$ , is applied between two electrodes separated by a distance  $d$  is shown in Figure 7.

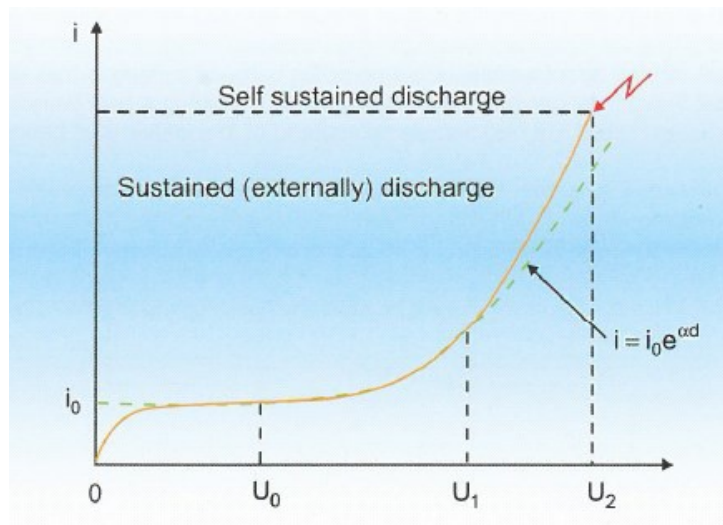


Figure 7: Voltage versus current characteristic of the discharge (Maruvada, 2011)

Referring to Figure 7 , the stages are (Maruvada, 2000):

#### The dark discharge

For voltages below  $U_0$  (saturation voltage) the current increases linearly and then saturates gradually as it approaches  $U_0$ . At lower voltages the electric field sweeps out the ions and electrons created by ionisation from background radiation. The background radiation originates from cosmic rays, radioactive minerals or other sources. The rate of the creation of free electrons at these field levels exceeds the rate at which they cross the gap, giving rise to a linear voltage - current relationship. Avalanching does not occur.

#### Saturation region

If the potential difference between the electrodes is further increased beyond  $U_0$ , eventually all the available electrons and ions are swept away and the current consequently saturates. The current remains constant while the voltage is increased. The amplitude of the current depends linearly on the radiation source strength.

#### Townsend discharge

As the voltage is increased above  $U_0$ , the electric field in the gap is sufficiently large giving rise to excitation and ionisation by electron collision and to field intensified ionisation leading to the formation of electron avalanches. The current starts increasing exponentially i.e.

$$I = I_0 e^{\alpha d} \tag{6}$$

- where

$U_0$  is the saturation voltage

$I_0$  is the saturation current at  $U_0$

$d$  is the distance between the cathode and the anode

$\alpha$  is the ionisation coefficient (Maruvada, 2000)

A corona discharge occurs in regions of high electric field near sharp points, edges, or wires in gases prior to electrical breakdown. The electrical field is the dominant parameter, rather than the potential difference between the electrodes. If the corona currents are high enough, corona discharges can be visible to the naked eye and resemble a glow (Maruvada, 2011). Corona discharges are also called partial discharges as they do not occupy the entire distance between the two electrodes but are present only in the region of a high electrical field. (Bouchacourt, et al., 2003).

Above a certain voltage  $U_1$ , the current increases more rapidly than the exponential relationship in Equation (6). This results in electrical breakdown at  $U_2$ . Electrical breakdown occurs in the Townsend region when the ions reaching the cathode have sufficient energy to generate secondary electrons. The creation of secondary electrons at the cathode surface makes the discharge process independent of the source of the initial electrons and leads to breakdown of the gap (Maruvada, 2000). If the current supply is too low, the discharge will remain in the corona region with small corona points or brush discharges being visible at the electrodes. The breakdown voltage for a particular gas and electrode material depends on the product of the pressure and the distance between the electrodes. The plasma gas emits light since the electron energy and number density are high enough to generate excited gas atoms by collisions. These excited gas atoms will eventually relax to their ground state through the emission of photons (Bouchacourt, et al., 2003).

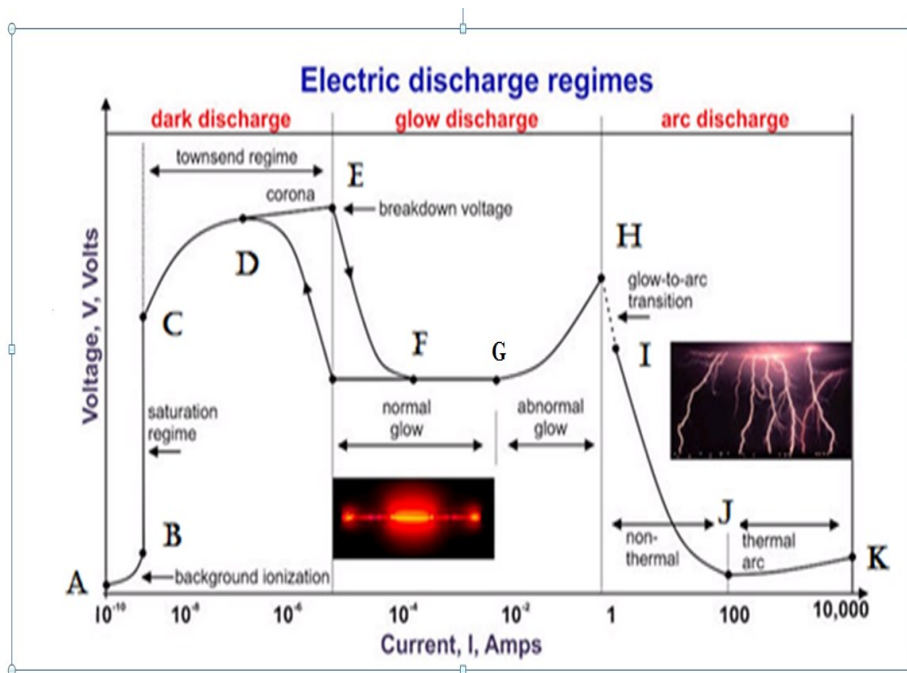


Figure 8 : Voltage versus current characteristic for a gas discharge (Bouchacourt, et al., 2003)

For a high discharge current, now referring to Figure 8, after a discontinuous transition from E to F, the gas enters the normal glow region (F - G), in which the voltage is almost independent of the current. As the current increases from F to G, the fraction of the cathode occupied by the plasma increases, until the plasma covers the entire cathode surface at point G. Once the whole surface of the cathode is covered by the discharge, the only way the total current can increase further is to drive more current through the cathode by increasing the current density. (Bouchacourt, et al., 2003).

This stage where the voltage increases significantly with increasing total current (G-H) is the abnormal glow region. As the voltage and cathode current density increase, the average ion energy impacting the cathode surface also increases. The bombardment with ions ultimately heats the cathode. Once the cathode is hot enough to emit electrons thermionically, the discharge will change to an arc discharge (Bouchacourt, et al., 2003).

At point H, the electrodes become sufficiently hot that the cathode emits electrons thermionically. If sufficient current is supplied to the discharge it will undergo a glow-to-arc transition, (H-I). The arc region, from I through K is one where the discharge voltage decreases as the current increases, until large currents are achieved at point J. Thereafter the voltage increases slowly with increasing current (Bouchacourt, et al., 2003).

### 2.1.7 Types of corona and their spectra

Figure 9 is a typical spectrum of light emitted by a corona discharge in air. The corona produces mainly low intensity UV radiation at the lower wavelength end of the solar spectrum. Outside the solar blind region many peaks emerge as shown in Figure 9.

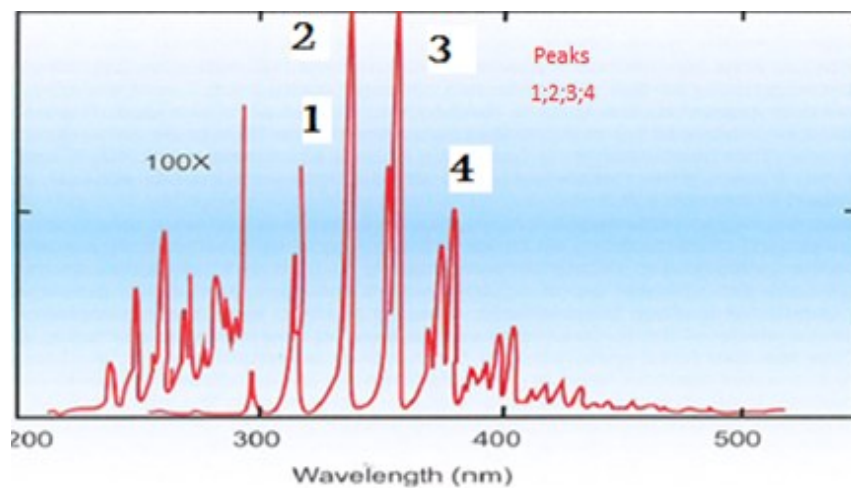


Figure 9: DC corona light spectrum (Maruvada, 2000)

There is DC, AC and HF corona according to the nature of the supply voltage and unipolar (positive or negative) corona according to the polarity of the active electrode (Peek, 1929).

For AC supply voltages, as the voltage goes above the corona onset value in each of the positive and negative half cycles, different corona modes (i.e. burst corona, onset streamer, pulse-less glow and breakdown streamer) occur. The discharge processes for AC differ from DC due to the residual space charge with the same polarity as that of the previous half cycle (Peek, 1929).

For AC supply voltages:

When the conductor is positive with respect to ground, an electron avalanche moves rapidly into the conductor leaving the heavy positive-ion charge cloud, which drifts away. The rapid movement of electrons gives the steep front of the current pulse, while the drift of positive ions gives the slow tail of the current pulse. When the conductor is negative with respect to ground, an electron avalanche moves away from the energized conductor and the heavy positive ions move towards the conductor. Since the heavy positive ions are moving towards the higher electric field, their motion

is very rapid which gives rise to a much steeper current pulse. Due to the rapid moment of the electrons from the conductor surface, the electric field regains its original value at the conductor surface more quickly than in the case of the positive polarity. Thus the negative corona current pulses are lower in amplitude and shorter in rise and fall times as compared to positive corona current pulses. The negative corona current pulses have higher repetition rates than the positive corona current pulses (Peek, 1929).

A published spectrum for AC corona is shown in Figure 10:

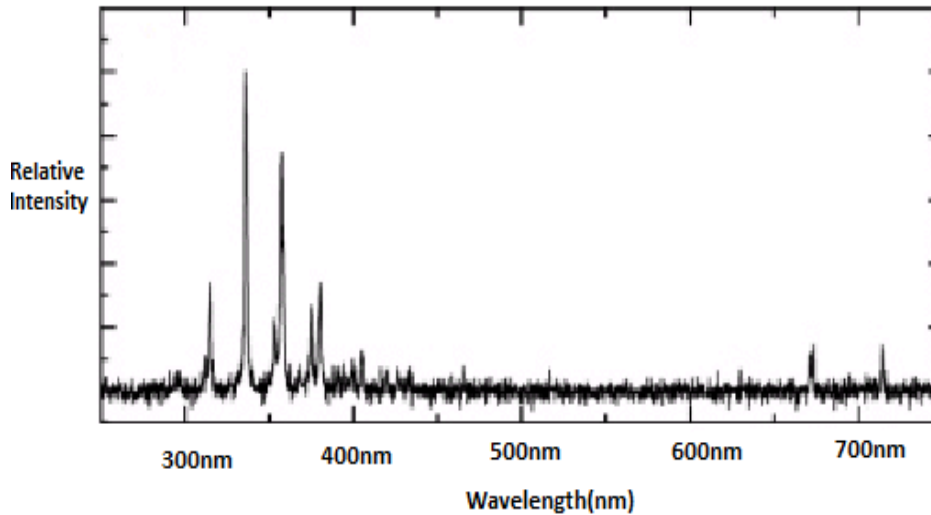


Figure 10: AC corona spectrum (Chen, 1998)

From Figure 10 the spectral lines are mainly in the UV range. The most intense emissions are in the range of 300 nm – 440 nm. This is similar to the spectra of DC corona. Between the ranges the 250 nm – 300 nm, only one strong emission line emerges. With increasing voltage, the emission intensity increases and more emission lines emerge. More emission lines specifically in the 400 nm – 700 nm emerge similar to the DC spectra shown in Figure 11 . Lawrence and Dunnington (Loeb, 1939) demonstrated that at exceedingly high local electric fields i.e. order of  $>10^5$  kV/cm peak shifting and spectral broadening occurs. This is known as the Stark Effect.

Two processes may result in the broadening of a spectral line:

- Collisions between molecules (Pressure broadening).
- Differences in the molecule thermal velocities (Doppler broadening).

Raising the applied voltage increases the amplitude of the spectra and longer wavelength spectra emerge as shown in Figure 11 (Shixiu, 1998).

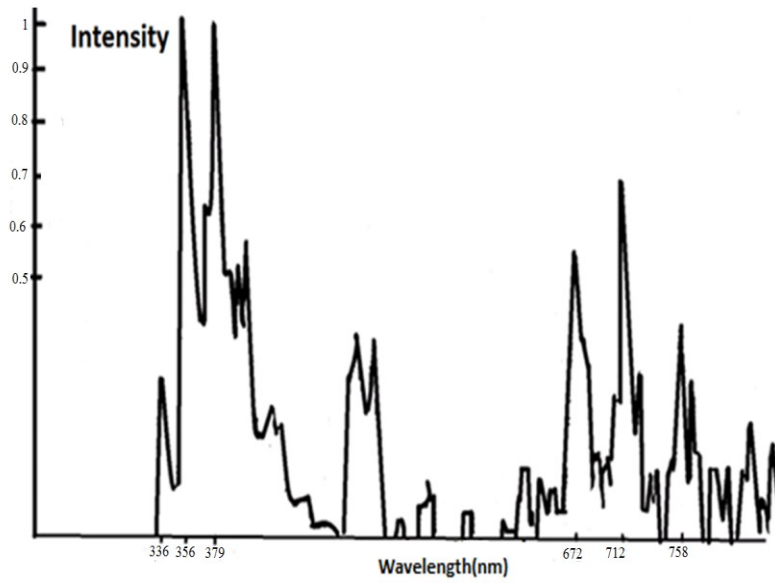


Figure 11: DC corona spectra showing increased intensity and longer spectral wavelength (Shixiu, 1998)

Furthermore there are spectra beyond 730 nm arising as shown in Figure 12.

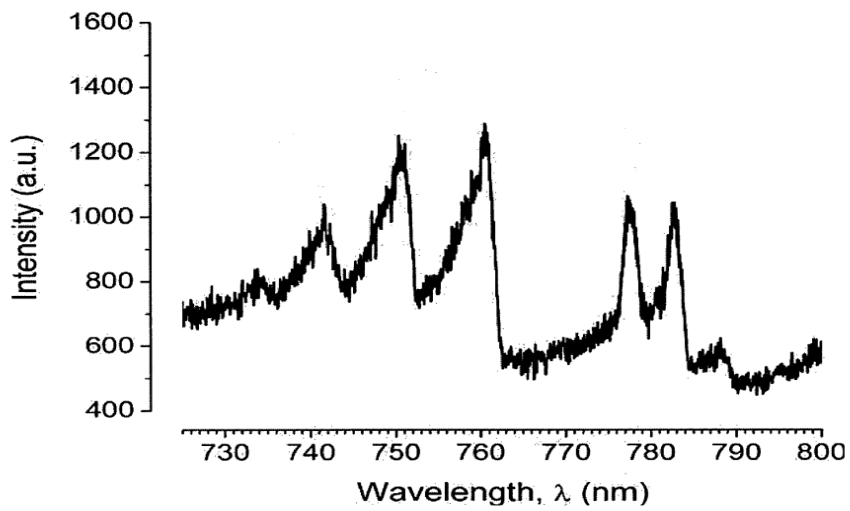


Figure 12: Spectra visible beyond 730 nm



The emergence of near infrared light may imply a rising of gas temperature. Furthermore many small peaks emerge beside big peaks which indicates that there are more and more molecules whose vibrational - rotational levels has been excited. (Shixiu, 1998).

The corona emission in air is shown in Figure 13.

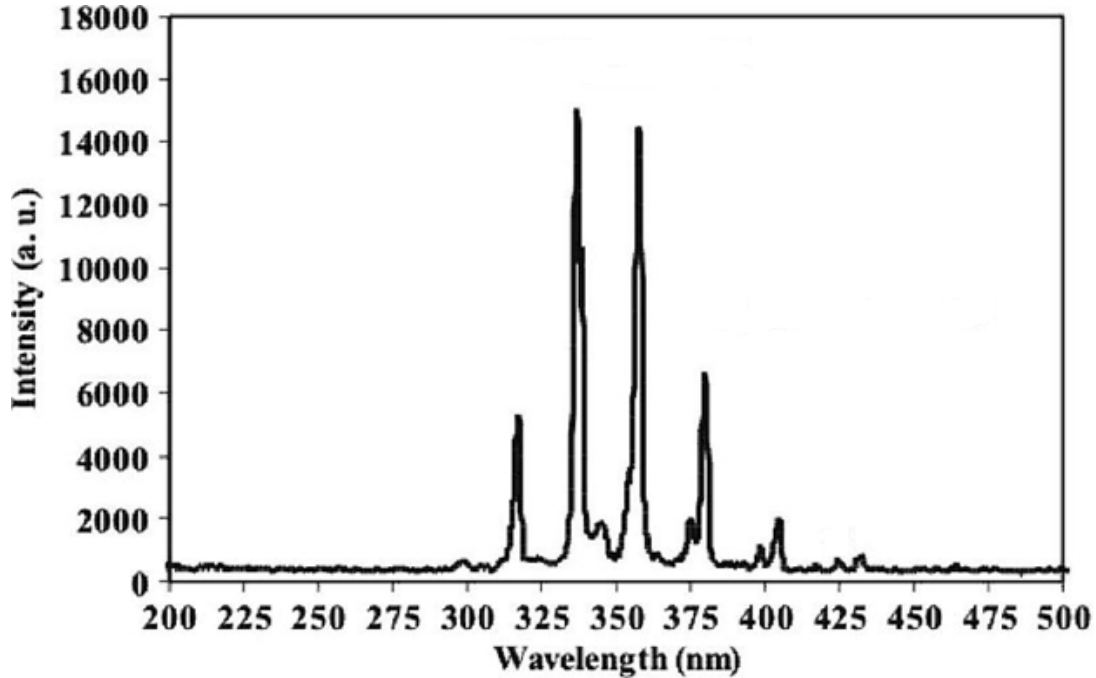


Figure 13: Corona emission in air (Shimizu, 2011)

## 2.1.8 Parameters of corona

### 2.1.8.1 Corona onset gradient

The onset of corona is classified as the initiation of a self-sustaining discharge near the conductor surface and occurs when the conductor surface voltage gradient reaches a critical value. The corona onset gradient is a function of the conductor diameter and its surface condition as well as of the ambient temperature and pressure (Maruvada, 2000).

In general the corona onset gradient  $E_c$  is expressed by Peek's law as (Maruvada, 2000):

$$E_c = mE_0\delta\left(1 + \frac{K}{\sqrt{\delta r}}\right) \quad (7)$$

- where

$E_0$ ,  $K$  depend on the nature of the applied voltage and geometry

$r$  is the conductor radius, in cm

$m$  is the surface irregularity factor

The values of  $m$  lie between 0,8 and 1. For polished and smooth clean conductors the surface irregularity factor is 1, for roughened, dirty or weathered wires the roughness factor is between 0,93 and 0,98. The value of  $m$  for stranded conductors is 0,75 and 0,85 depending on the ratio of strand to conductor diameter. Practical stranded conductors may have nicks and scratches which reduces  $m$  to 0,6 and 0,8. The presence of water drops or heavy fog, snowflakes etc. reduces  $m$  to 0,3 and 0,6 (Maruvada, 2000).

Figure 14 shows the effect of varying temperature and conductor radius on the corona onset gradient.

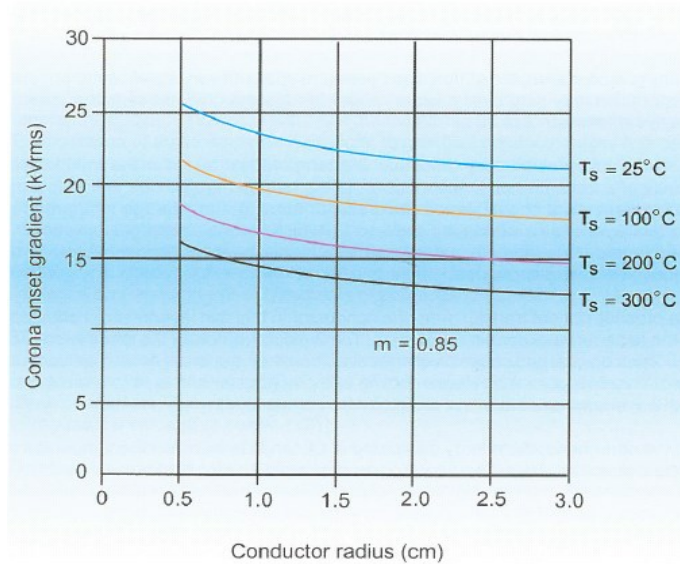


Figure 14: Effect of conductor surface temperature and conductor radius on the corona onset gradient (Maruvada, 2011)

Figure 15 shows the effect of altitude and conductor radius on the corona onset gradient.

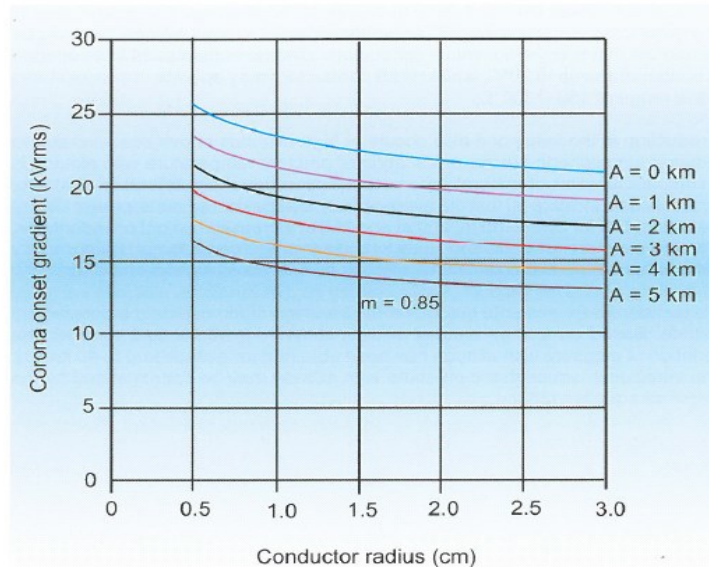


Figure 15: Effect of altitude and conductor radius on the corona onset gradient (Maruvada, 2011)

The air density correction factor is (Maruvada, 2000):

$$\delta = \frac{273 + t_0}{273 + T} \cdot \frac{p}{p_0} \quad (8)$$

- where

T is the temperature, in °C, and p is the pressure of ambient air, in cmHg  
 $t_0$  and  $p_0$  are reference values. Usually  $t_0=25^\circ\text{C}$  and  $p_0=76\text{ cmHg}$   
 Substituting  $t_0=25^\circ\text{C}$  and  $p_0=76\text{ cmHg}$

$$\delta = \frac{3.92p}{273 + T} \quad (9)$$

The empirical constants for ac, according to (Peek, 1929) are  $E_0=29.8\text{kV}_{\text{peak}}/\text{cm}$  or  $21\text{kV}_{\text{rms}}/\text{cm}$  and  $K=0.301$ . The corresponding values for DC according to Whitehead are  $E_0=33.7\text{kV}/\text{cm}$  and  $K=0.24$  for positive polarity and  $E_0=31\text{kV}/\text{cm}$  and  $K=0.308$  for negative polarity. The constant K for negative polarity DC (Whitehead) is the same for AC indicating that the AC corona onset occurs during the negative half-cycle of AC (Maruvada, 2000).

The equations described above were derived from experiments on smooth conductors with diameters smaller than that of practical transmission lines. Furthermore the diameter of the outer cylinder was smaller which influenced the measured ac corona onset gradients. In practical applications it has been noted that the corona onset gradient is much higher than measured values (Maruvada, 2011). It is noted that the corona onset gradient remains the same for different electrode shapes that have the same mean curvature or same equivalent radius.

Figure 16 shows the measurements made of the corona onset gradient as a function of the equivalent radius ( $r_{eq}$ ).

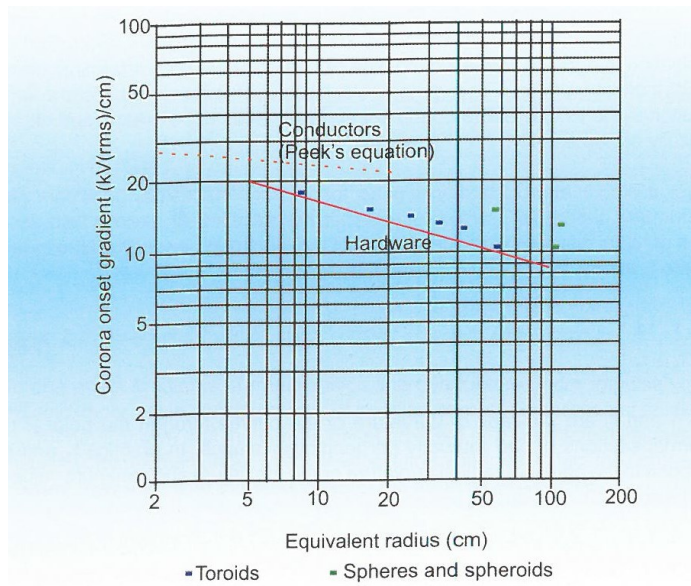


Figure 16: Corona onset gradients of hardware electrodes (Maruvada, 2011)

### 2.1.8.2 Corona inception voltage

The corona inception voltage is the voltage at which the electric field at the surface of the conductor equals the breakdown strength of air. The voltage can be calculated for a coaxial geometry, if the conductor is smooth and solid by (Singh, 2003):

$$V_D = rE_0\delta \ln\left(\frac{d}{r}\right) \quad (10)$$

- where

$$\delta = \frac{3.92p}{273 + T}$$

r is the radius of the wire, in cm

d is the distance between electrodes, in cm

p is pressure, in cmHg

T is temperature, in °C

The value of the potential gradient at which ionisation takes place under normal temperature (25°C) and pressure (76 mmHg) and without impurities is  $E_0 = 21, 1 \text{ kV}_{\text{rms}}/\text{cm}$ . More generally, due to the irregularity of the surfaces, dust and dirt, there is further reduction in the breakdown voltage. Allowing the surface irregularity factor, m of the wire and the air density correction factor, the corona inception voltage will be (Singh, 2003):

$$V_D = rE_0m\delta \ln\left(\frac{d}{r}\right) \tag{11}$$

The voltage above is valid for fair weather conditions. However in the case of foul and bad weather conditions, the visual corona inception voltage decreases considerably (Singh, 2003).

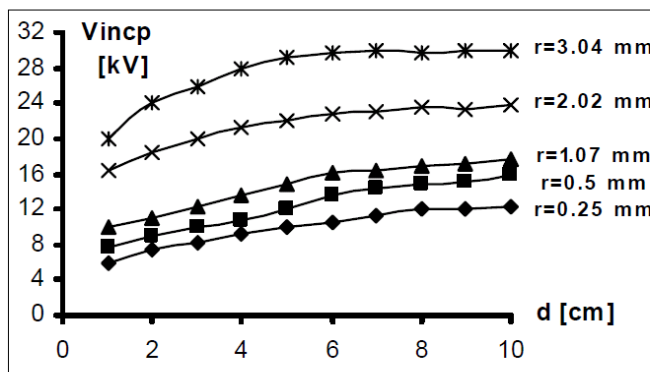


Figure 17: Corona inception voltage for rod-plane versus gap length with various rod radii, r (Javadi, et al., 2010)

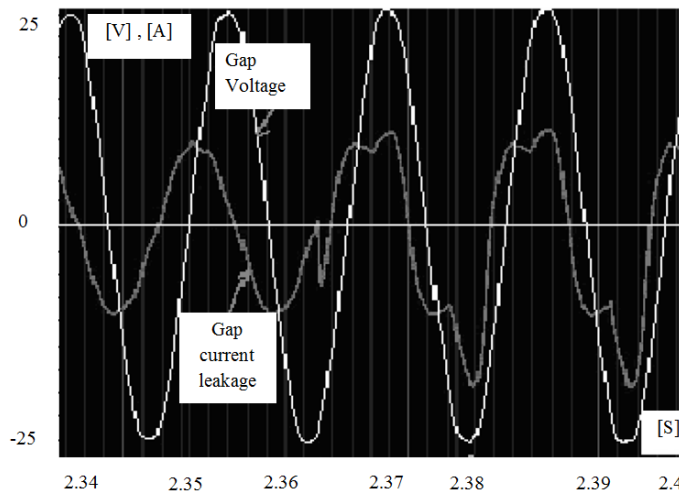


Figure 18: Gap voltage and corona current wave shape for a rod plane gap (r=2.48mm and d=4cm) (Javadi, et al., 2010)

### 2.1.8.3 Visual corona inception voltage

The visual corona inception voltage is the minimum voltage at which the corona becomes visible. In parallel conductors it is higher than the corona inception voltage (Singh, 2003).

The visual corona inception voltage is given by (Singh, 2003):

$$V_V = E_0 \delta m_v r \left(1 + \frac{K}{\sqrt{r\delta}}\right) \ln \frac{d}{r} \text{ kV(rms)} \quad (12)$$

$$V_V = V_D \left(1 + \frac{K}{\sqrt{r\delta}}\right) \text{ kV(rms)} \quad (13)$$

- where

$$\delta = \frac{3.92p}{273 + T}$$

r is the radius of the wire, in cm

d is the distance between electrodes, in cm

p is pressure, in cmHg

T is temperature, in °C

$E_0$  is the gradient for the visual corona inception voltage, in kV/cm

$m_v$  is different from the roughness factor, m.

K depend on the nature of the applied voltage and geometry.

The amount of corona produced by a transmission line is a function of the voltage of the line, the diameter of the conductors, the locations of the conductors in relation to each other, the elevation of the line above sea level, the condition of the conductors and the local weather conditions. Large-diameter conductors have lower electric field gradients at the conductor surface and hence less corona than smaller conductors. Irregularities (such as nicks and scrapes on the conductor surface or sharp edges on suspension hardware) concentrate the electric field at these locations and thus increase the electric field gradient and the resulting corona at these spots. Similarly foreign objects on the conductor surface such as dust or insects can cause irregularities on the surface that are a source for corona. Corona also increases at higher elevations where the density of the atmosphere is less than at sea level (Maruvada, 2011).

The factors that affect corona loss are (Peek, 1929):

#### 1. Atmospheric factors

- Corona loss is inversely proportional to pressure.
- Corona loss is increased by dust and dirt on the conductor.
- Corona loss is increased by rain, snow, hail and fog (bad weather conditions).
- Corona loss is proportional to temperature.

#### 2. Electrical Factors (Peek, 1929)

- If the frequency is higher, corona losses increase. The corona loss is less in DC transmission than in AC transmission.
- If the supply voltage is high, the corona loss increases. In a low voltage line the corona is absent due to an insufficient field to maintain the self-sustained ionisation.

#### 3. Conductor factors (Peek, 1929)

- Corona loss is a function of the conductor configuration.
- Corona loss decreases with increased conductor diameter.
- Polished surfaces result in less corona loss, unpolished surfaces result in more corona loss.

- Oxidation and salt contribute to an increase in corona loss.
- Corona loss decreases if conductor bundles are used: the effective radius is increased which reduces the electric field and corona loss.
- Corona loss is reduced if the conductor is hot since there is a reduced condensation of fog or dew.
- Corona loss increases with reduced conductor spacing.

#### 2.1.9 Effects of corona

##### 1. Audible Noise

During corona activity, transmission lines (primarily those rated at 345 kV and above) can generate a small amount of audible noise. This audible noise can increase during inclement weather conditions. Water drops may collect on the surface of the conductors and increase corona activity so that a crackling or humming sound maybe heard near a transmission line (Maruvada, 2011).

##### 2. Gaseous Effluents

Corona activity in the air can produce very tiny amounts of gaseous effluents: ozone and NO<sub>x</sub> (NO<sub>x</sub> gases can come from combustion where nitrogen in the air becomes oxidized) (Maruvada, 2011).

##### 3. Induced Currents

The streamers generated during corona discharge, transport electric charge into the surrounding air during the discharge cycle. These moving charges contribute directly to the radio frequency noise. They also cause currents to be induced on communication lines (Maruvada, 2011). Since the charge is moved by a time varying electric field, it is equivalent to a current pulse so when a communication line passes near a HV transmission line, if the frequency of the radiated EM wave due to corona matches with that of the transmitted signal on the communication line, then the communication signal may get distorted. To mitigate this effect, the communication line should pass at a safe distance away from the transmission line (Maruvada, 2011).

#### 2.1.10 Methods to reduce corona

Corona can be avoided by minimizing the electric field gradient. This is accomplished by using good high voltage design practices, i.e. maximizing the distance between conductors that have large voltage differentials, by using conductors with large radii and by avoiding parts that have sharp points or edges.

Corona rings are meant to reduce electrical fields. The typical line voltage where corona rings are applied is 150 kV and higher. A corona ring could surround the energized end of a transformer bushing. Corona rings function by electrically shielding the bushing terminal and connections. This reduces the voltage gradient to a level below the ionizing gradient of the surrounding air. A corona ring could also help to smooth the voltage profile along an insulator preventing concentration of over-stresses (Loeb, 1939).

The corona inception voltage can sometimes be increased by using a surface treatment such as a semiconductive layer. However if air is the insulator, then geometry is the critical parameter to focus on. Corona produced on a transmission lines can be reduced by the design of the transmission line and the selection of hardware and conductors used for the construction of the line. For instance the use of conductor hangers that have rounded rather than sharp edges and no protruding bolts with sharp edges will reduce corona (Loeb, 1939).

### 2.1.11 Presently used corona detection methods

Technologies to detect corona, short duration arcing or sustained arcing are based upon the emissions from the source. The technologies to reliably detect and locate discharges include the following (Bouchacourt, et al., 2003):

- A daylight corona camera which is used in full light and a night vision corona camera used in low light.
- Audible noise or ultrasound.
- Electromagnetic radiation.
- Infrared cameras (specifically for sustained arcing).
- Electric-field measurement (specifically for corona).
- Visual observation (specifically for corona).

Both acoustic emission and radio interference voltage (RIV) measurement methods are sensitive to background noise. They cannot be used to determine the precise location of corona (Bouchacourt, et al., 2003). Electric field measurements yield erroneous results in the presence of moisture and require deployment from the tower which is not convenient. For all the above reasons, visual observation by knowledgeable personnel either from ground or helicopters remained the most effective method for corona inspection until the use of UV cameras (Bouchacourt, et al., 2003). Special UV cameras to detect corona in daytime are increasingly being used by the utilities for periodic inspections. These cameras can provide information on the exact location of corona.

In the following section the CoroCam will be discussed further.

#### 2.1.11.1 CoroCam

Electricity utilities make use of a number of inspection tools to survey their transmission lines and electrical distribution equipment. IR, visible and UV cameras are the latest visual diagnostic tools available to utilities to identify potential failures on electrical equipment.

An infrared camera locates high temperature problem areas (hot spots) which could result in a mechanical failure and consequently a power failure. A UV camera locates corona problem areas on hardware and insulators that could result in a flashover and hence in a power outage. Such techniques include imaging that takes either an IR or a UV image of the insulator. Such images may indicate some changes to either the external (visible) components of the insulator or to the internal (non-visible) components that may impact the long-term integrity of the insulator. IR and UV imaging are the preferred diagnostic techniques for inspecting composite insulators. Presently all three techniques appear as stand-alone instruments used by different utility inspection and maintenance teams under different circumstances. By combining the three inspection techniques into one instrument, significant savings can be achieved i.e. MultiCam (Vosloo, et al., 1997).

The wavelengths of the EM spectrum are divided into different categories as illustrated in Figure 19.

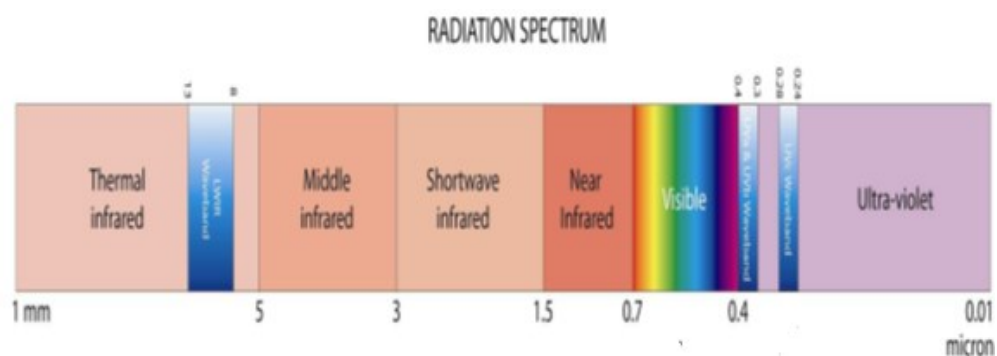


Figure 19: Radiation spectrum (Vosloo, et al., 1997)

The x-ray domain for short wavelengths with powerful penetrable photons, the visible spectrum where humans can observe objects and the long wavelength radio waves where communication waves are transmitted and received. The multi-spectral imager (MultiCam) explores the UV wavelengths between 200nm to 280nm, the visible wavelengths of 400nm (dark blue) to 780nm (red) and the IR wavelengths of 8µm to 12µm (Vosloo, et al., 1997). Corona on electrical equipment radiates energy in the form of light, mainly in the UV band of the EM spectrum (300-400nm) with spectral peaks at 340 and 360nm as shown in Figure 2.

## 2.2 Fraunhofer lines

Solar radiation is influenced by the following factors (Averill, 2007):

1. Seasonal variation
2. Location
3. Time of day
4. Where one is looking

The extent to which radiation is blocked by the aerosols, water vapour, clouds, ozone etc. in the atmosphere affects the intensity of the solar radiation reaching the earth. The less opaque the atmosphere is i.e. transparent, the higher the intensity of extra-terrestrial solar radiation reaching the Earth's surface (Averill, 2007). Spectroscopic observations enable us to investigate light divided into the many wavelengths using a prism or a diffraction grating.

A diffraction grating is an optical component with a periodic structure, which splits and diffracts light into several beams traveling in different directions. A diffraction grating disperses an incident beam. The directions of these beams depend on the slit spacing and the wavelength of the light. This makes the grating act as a dispersive element (Wako, 2011). The sun emits light primarily in the visible spectrum, but it also emits at other wavelengths, as illustrated in Figure 20 (Bird, et al., 1983). Longer wavelengths have less energy (for instance IR) than shorter ones such as visible light or UV. This is shown in Figure 20 by the spectral irradiance.

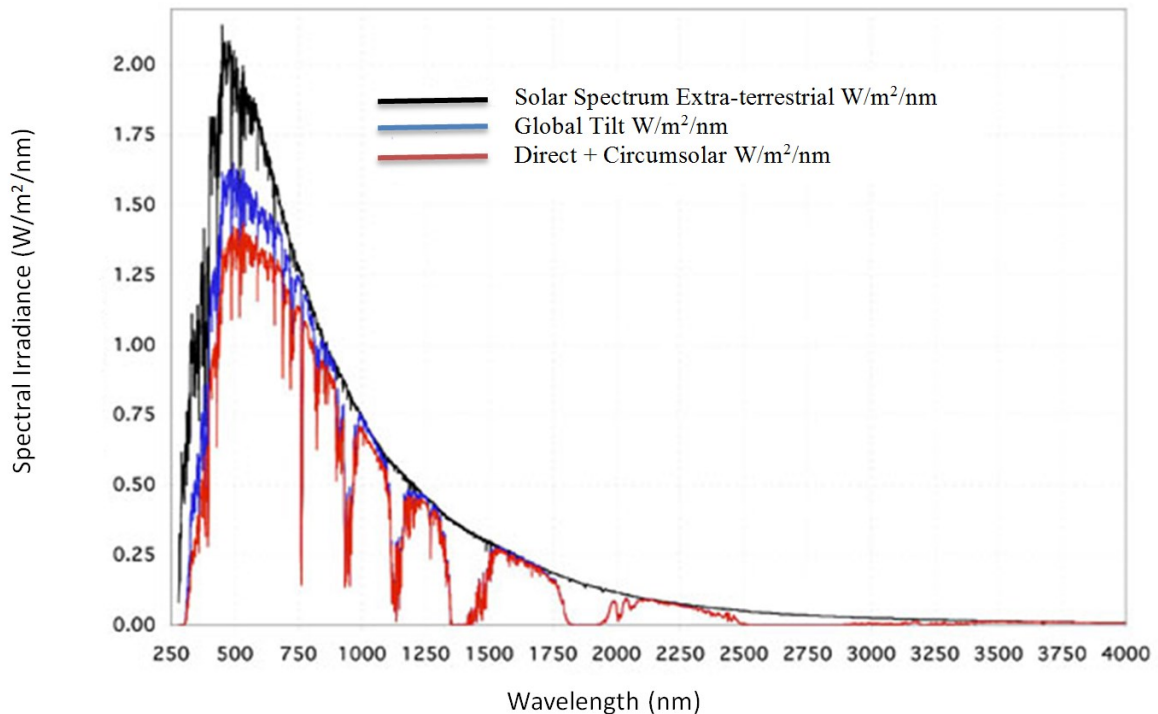


Figure 20: Solar spectrum generated in SMARTS (Bird, et al., 1983)



Closer inspection shows that the solar spectrum is interrupted by a large number of narrow dark lines as shown in Figure 21.

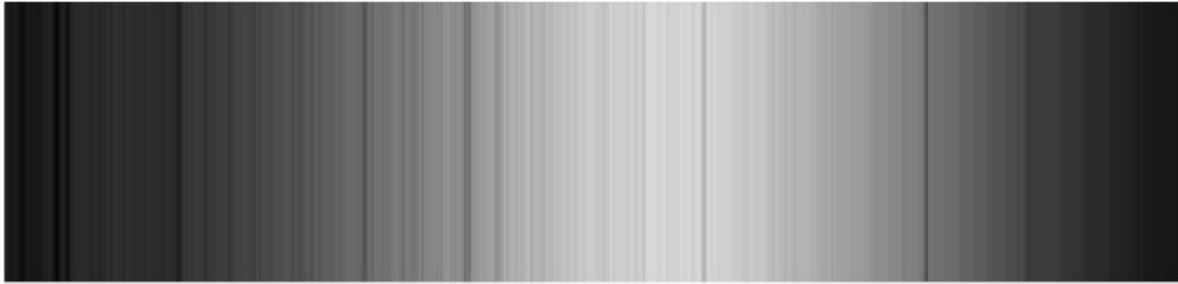


Figure 21: Spectrum showing absorption lines (Averill, 2007)

These lines represent wavelengths of light that have been removed by gases present in the outer layers of the sun. These lines of the solar spectrum are called absorption lines or Fraunhofer lines (Walloston, 1802).

The following section will describe the physics behind Fraunhofer lines, how Fraunhofer lines are measured and why they could conceivably be significant in corona detection.

### 2.2.1 The Fraunhofer lines

Fraunhofer lines are a set of spectral lines named after the German physicist Joseph von Fraunhofer (1787–1826). The lines were originally observed as dark features (absorption lines) in the optical spectrum of the sun. The Fraunhofer lines are typical spectral absorption lines. Each line represents the net absorption of photons by a particular atom or molecule and the transition of an electron between energy levels in an atom. Each element has a distinct pattern of absorption lines (Wako, 2011) (Walloston, 1802).

An example of solar-type spectra in the UV band is shown in Figure 22. The major broad-band Fraunhofer absorption lines are shown in red (Kingsley, 1990).

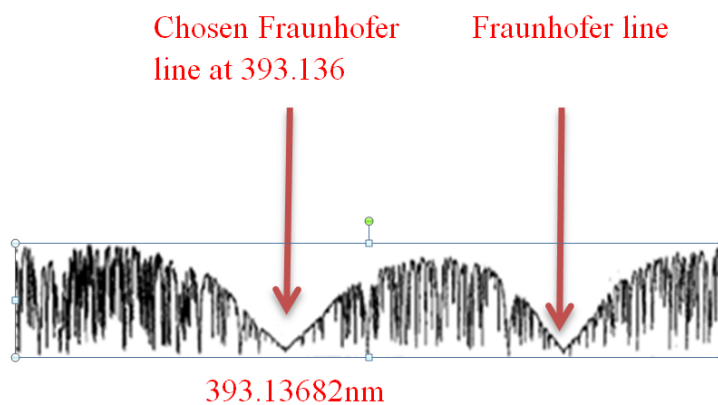


Figure 22: Solar spectra in the ultra-violet region demonstrating the major broad-band Fraunhofer lines (Kingsley, 1990)

Fraunhofer mapped over 570 lines and assigned the features with the letters A through K and weaker lines with other letters (Wako, 2011). The dominant Fraunhofer lines are shown in Table 1. The highlighted wavelength in the table is the selected Fraunhofer line for further processing. The intensity within the Fraunhofer line at this wavelength is much lower when compared with the other Fraunhofer lines which implies a better SNR is achievable.

Table 1: The Dominant Solar Fraunhofer lines (Bird, et al., 1983)

Wavelength(nm))	FWHM(nm)	FWHM(GHz)	Element
333.6689	0.0416	112.1	Mg I
341.4779	0.0816	209.9	Ni I
343.3579	0.0492	125.2	Ni I <sup>2</sup>
344.0626	0.1243	315.0	Fe I
344.1019	0.0634	160.6	Fe I
344.3884	0.0655	165.7	Fe I
344.6271	0.0470	118.7	Ni I
345.8467	0.0656	164.5	Ni I
346.1667	0.0758	189.8	Ni I
347.5457	0.0622	154.5	Fe I
347.6712	0.0465	115.4	Fe I <sup>2</sup>
349.0594	0.0830	204.4	Fe I
349.2975	0.0826	203.1	Ni I
349.7843	0.0726	178	Fe I
351.0327	0.0489	119.1	Ni I
351.5066	0.0718	174.3	Ni I
352.1270	0.0381	92.2	Fe I
352.4536	0.1271	306.9	Ni I
355.4937	0.0404	95.9	Fe I
355.8532	0.0485	114.9	Fe I <sup>2</sup>
355.5936	0.0990	233.6	Fe I
356.6383	0.0458	108	Ni I
357.0134	0.1380	324.8	Fe I
357.8693	0.0488	114.3	Cr I
358.1209	0.2144	501.5	Fe I
359.3495	0.0436	101.3	Cr I
360.8869	0.1046	240.9	Fe I
361.8777	0.1410	323.0	Fe I
361.9400	0.0568	130.1	Ni I
363.1475	0.1364	310.3	Fe I <sup>2</sup>
364.7851	0.0970	218.7	Fe I <sup>2</sup>
367.9923	0.0448	99.2	Fe I <sup>2</sup>
368.5196	0.0275	60.7	Ti II
370.5577	0.0562	122.8	Fe I
370.9256	0.0573	124.9	Fe I <sup>2</sup>
371.9947	0.1664	360.7	Fe I
373.4874	0.3027	651.0	Fe I
373.7141	0.1071	230.1	Fe I
374.5574	0.1202	257.0	Fe I <sup>2</sup>
374.8271	0.0497	106.1	Fe I
374.9495	0.1907	406.9	Fe I
375.8245	0.1647	349.8	Fe I
375.9299	0.0334	70.9	Ti II
376.3803	0.0829	175.6	Fe I
376.7204	0.0820	173.3	Fe I
378.7891	0.0512	107.1	Fe I
379.5012	0.0547	113.9	Fe I <sup>2</sup>
380.6718	0.0209	43.3	Fe I <sup>2</sup>
381.5851	0.1272	262.1	Fe I
382.0436	0.1712	351.9	Fe I
382.5891	0.1519	311.3	Fe I
382.7832	0.0897	183.7	Fe I

Wavelength(nm))	FWHM(nm)	FWHM(GHz)	Element
382.9365	0.0874	178.8	Mg I
383.2310	0.1685	344.2	Mg I
383.4233	0.0624	127.3	Fe I
383.8302	0.1920	391.0	Mg I
384.0447	0.0567	115.3	Fe I
384.1058	0.0517	105.1	Fe I <sup>2</sup>
384.9977	0.0608	123.1	Fe I
385.6381	0.0648	130.7	Fe I
385.9922	0.1554	312.9	Fe I
387.8027	0.0555	110.7	Fe I
388.6294	0.0920	182.7	Fe I
389.9719	0.0436	86.0	Fe I
390.2956	0.0530	104.4	Fe I <sup>2</sup>
390.5532	0.0816	160.5	Si I
392.0269	0.0341	66.6	Fe I
392.2923	0.0414	80.7	Fe I <sup>2</sup>
392.7933	0.0187	36.4	Fe I
393.0308	0.0108	21.0	Fe I
393.3682	2.0253	3926.6	Ca II <sup>2</sup>
394.4016	0.0488	94.1	Al I
396.1535	0.0621	118.7	Al I
396.8492	1.5467	2946.3	Ca II
404.5825	0.1174	215.2	Fe I
406.3605	0.0787	143.0	Fe I <sup>2</sup>
407.1749	0.0723	130.8	Fe I
407.7724	0.0428	77.2	Sr II <sup>2</sup>
410.1748	0.3133	558.7	H
413.2067	0.0466	71	Fe I <sup>2</sup>
414.3878	0.0466	81.4	Fe I
416.7277	0.0200	34.5	Mg I

Almost all of the lines observed in the light received from extra-terrestrial sources can be attributed to known elements (for example, many of the Fraunhofer lines in sunlight are associated with the element iron). It is clear that when light interacts with matter on very small scales, it does so in a discontinuous, stepwise manner (Walloston, 1802).

The structure of atoms is important to explain the formation of spectral lines.

There is a state of lowest energy, the ground state, which represents the “normal” condition of the electron as it orbits the nucleus. There is a maximum energy that the electron can have and still be part of the atom. Once the electron acquires more than that maximum energy, it is no longer bound to the nucleus, and the atom is said to be ionized. An atom having fewer (or more) than its normal complement of electrons and hence a net electrical charge is called an ion. Between those two energy levels, the electron can exist only in certain sharply defined energy states often referred to as orbitals. An atom is said to be in an excited state when an electron occupies an orbital other than its ground state. The electron now lies at a greater distance from its parent nucleus, and the atom has a greater amount of energy. The excited state with the lowest energy (i.e. the one closest to the ground state) is called the first excited state, that with the second-lowest energy the second excited state, and so on. Because electrons may exist only in orbitals having specific energies, atoms can absorb only specific amounts of energy as their electrons are boosted into excited states. Likewise, atoms can emit only specific amounts of energy as their electrons fall back to lower energy states. Thus, the amount of light energy absorbed or emitted in these processes must correspond precisely to the energy difference between two orbitals. This requires that light must be absorbed and emitted in the form of little “packets” of electromagnetic radiation or photons, each carrying a very specific amount of energy i.e.  $e = hc / \lambda$  (Walloston, 1802).

### 2.2.2 Measurement of the Fraunhofer lines

Radiation can be analysed with an instrument known as a spectroscope. This device consists of an opaque barrier with a slit in it, a prism and either a detector or a screen to allow the user to view the resulting spectrum (Education, n.d.). This is shown in Figure 23.

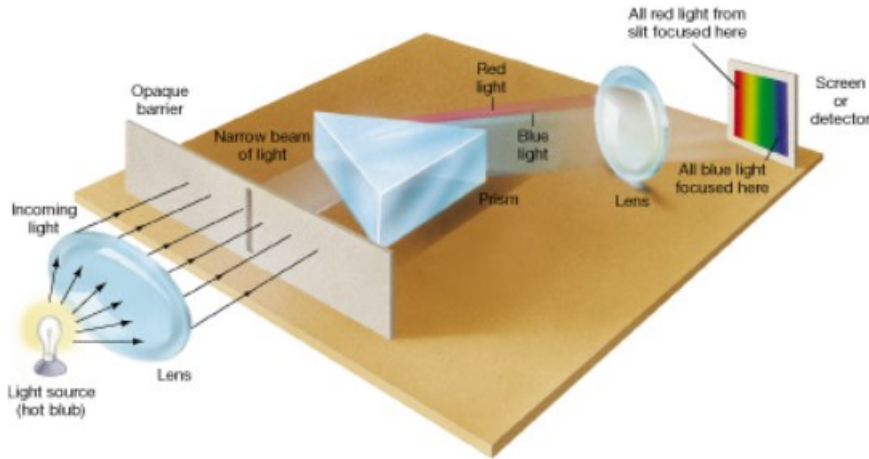


Figure 23: Diagram of a simple spectroscope (Averill, 2007)

A slit in the barrier allows a narrow beam of light to pass through. The beam then passes through a prism and is split into its component colours. A lens then focuses the light into a sharp image that is either projected onto a screen or analysed as it is passed through a detector (Education, n.d.). Spectroscopic observations enable us to investigate light divided into many wavelengths using a prism or a diffraction grating (Wako, 2011). When the light is dispersed more finely, the various wavelengths are distributed over a wider area on the detector. This means a higher spectral resolution which implies a reduced wavelength range since the size of the detector is limited (Wako, 2011).

### 2.2.3 Overlap between the Fraunhofer lines and the corona emission peaks

The major Fraunhofer lines are:

Table 2: Major Fraunhofer lines

Wavelength(nm)	Line due to
759.4	Telluric oxygen
686.7	Telluric oxygen
656.3	hydrogen, H
589.6	sodium
589.0	sodium
587.6	helium
527.0	iron and calcium
518.4	magnesium
486.1	hydrogen, H
430.8	iron (and calcium)
396.8	calcium
393.4	Calcium

The highlighted portion in Table 2 is the wavelength of the Fraunhofer line selected for further processing. One of the primary problems associated with observing corona UV radiation during daytime is that the wavelength corresponds directly to that of background solar radiation and therefore is masked from normal view (Czech, et al., 2011).

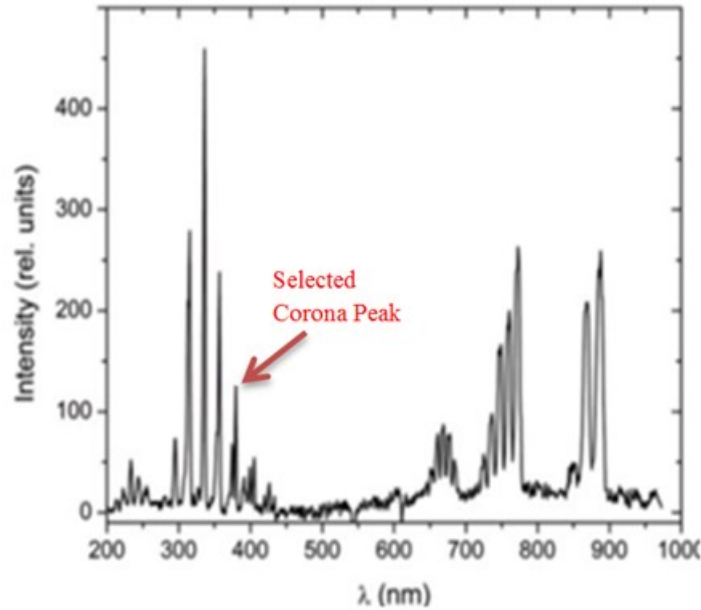


Figure 24: Corona spectrum (Schulze, et al., 2010)

From Figure 24 the strong emission bands lie between 300 and 400 nm. Fraunhofer lines are also present in this wavelength band.. Table 3 lists the overlap between the corona peaks and Fraunhofer lines.

Table 3: Overlap of corona and solar spectra at the Fraunhofer lines

Fraunhofer line (nm)	Line width (nm)	Corona peak (nm)
357.0134	0.1380	357.583
358.1209	0.2144	358.472
393.3682	2.0253	393.148
396.8492	1.5467	396.805

So in theory if it were possible to match the corona peaks with the Fraunhofer lines then conceivably it would be possible to measure corona discharges in the presence of solar radiation?

## 2.3 Signal Processing

### 2.3.1 Signal-to-noise ratio (SNR)

Two main types of measurement errors are recognized:

Systematic error- in which every measurement is consistently less than or greater than the correct value by a certain percentage or amount.

Random error - in which there are unpredictable variations in the measured signal from measurement to measurement (often called noise).

One of the fundamental problems in signal measurement is distinguishing the signal from the noise. The signal is the “important” part of the data (Haver, 1997). The quality of a signal is often expressed quantitatively as the signal-to-noise ratio (SNR). It is defined as the ratio of signal power to the noise power. A ratio higher than 1:1 (greater than 0 dB) indicates more signal than noise (Johnson, 2006):

$$\text{SNR} = \frac{P_{\text{signal}}}{P_{\text{noise}}} \quad (14)$$

- where P is the average power.

When the characteristics of the noise are known and are different from the signal, it is possible to filter the noise out.

### 2.3.2 Filters

Optical filters selectively transmit light in a particular range of wavelengths, while blocking the remainder. i.e. high-pass, low-pass or a band-pass filters. The pass-band may be narrow or wide. The transition between maximal and minimal transmission can be sharp or gradual (Murphy, et al., 1999).

Optical Filters can be broadly classified as absorption or dichroic, dependent upon their means of blocking unwanted wavelengths (Murphy, et al., 1999). Absorption filters transmit desired wavelengths by absorbing unwanted wavelengths as shown in Figure 25. These filters characteristically consist of dyed glass or pigmented gelatin resins. The ability of absorptive filters to attenuate light is based on the filter's physical thickness and the amount of dye or pigmentation present (Murphy, et al., 1999)

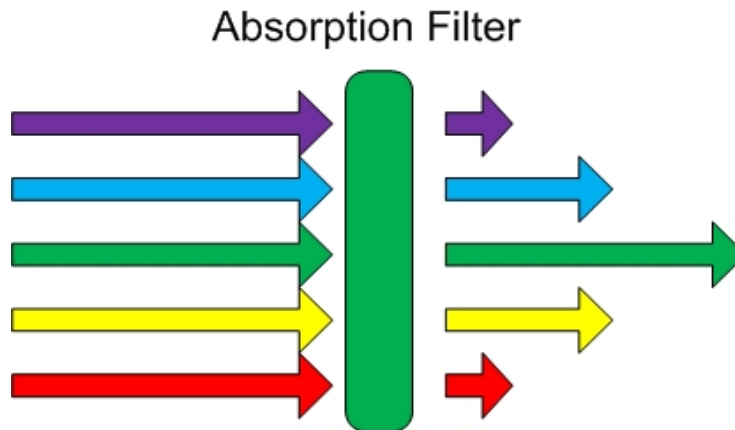


Figure 25: Absorption filter (Murphy, et al., 1999)

Dichroic filters are also known as interference filters. Interference filters filter light by rejecting all undesired wavelengths, allowing selected wavelengths to pass through. These filters are constructed using thin film technology by depositing several layers of dielectric film on one side of an optically flat piece of transparent glass as shown in Figure 26. When light strikes the coated side of the filter, the various layers of film transmit the desired wavelengths while reflecting and reducing the undesired ones (Murphy, et al., 1999). Segregation of the wavelengths stems from constructive and destructive interference at partially reflecting boundaries within the filter. Wavelengths within the pass-band gain optimal transmittance resulting from constructive interference while wavelengths outside the pass-band are cancelled due to destructive interference. The partially reflecting boundaries are formed by depositing films with alternating high and low refractive indices (Murphy, et al., 1999).

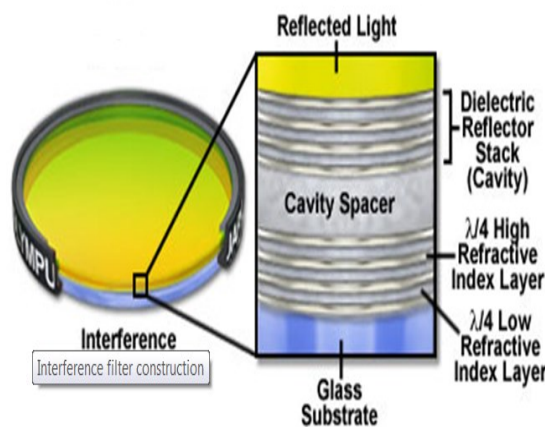


Figure 26: Anatomy of an interference filter (Murphy, et al., 1999)

Dichroic filters rely on the reflective cavities between the film layers to achieve their precise filtering. These cavities resonate with the desired wavelength frequencies while rejecting all others i.e. optical interference. Interference filters are capable of improved selectivity over absorption filters and are much more suitable for precision applications (Murphy, et al., 1999). Figure 27 is an example of a green interference filter.

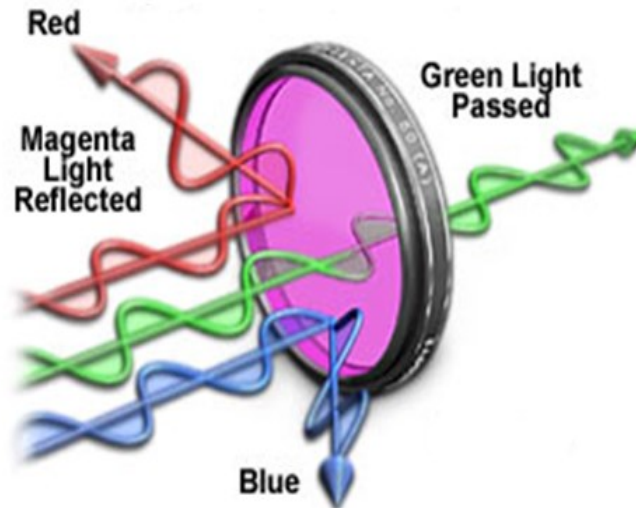


Figure 27: Green interference filter (Murphy, et al., 1999)

An interference filter should be illuminated by radiation collimated and perpendicular to its surface otherwise the central wavelength will be raised or lowered. Orientation of the filter is important specifically when directing the filter to or away from the source since this can have effects on the central wavelength (CWL) (Govire & Pete, 2007).

Percent transmission ( $\%T_\lambda$ ) is the most common unit used to quantitatively express how an optical filter transmits light. Percent transmission is measured at a particular wavelength (or wavelength range) and is the ratio of transmitted light intensity,  $I$  to incident light intensity,  $I_0$ , expressed as a percentage (Govire & Pete, 2007) :

$$\%T_\lambda = \frac{I}{I_0} \times 100 \quad (15)$$

The optical density is the amount of energy transmitted through the filter. A higher optical density indicates a lower transmission.

$$\%T_\lambda = 10^{-OD} \times 100 \quad (16)$$

- where OD is the optical density.

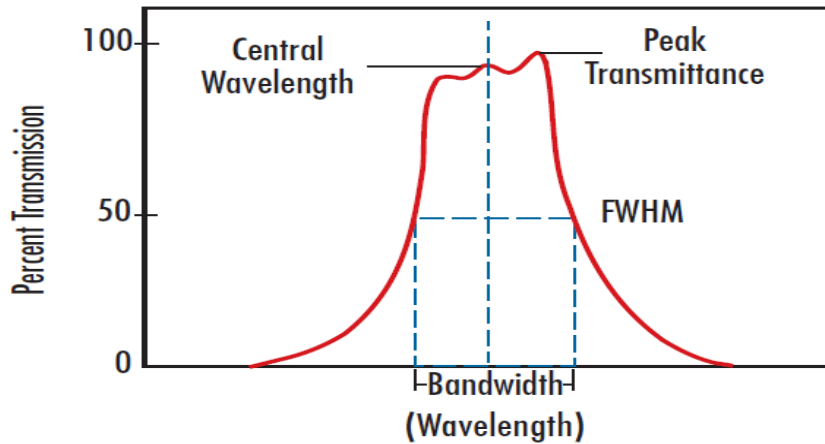


Figure 28: Band-pass filter transmission (Govire & Pete, 2007)

Band-pass filters are denoted by their CWL and FWHM. Figure 28 is a band-pass filter transmission curve. The center wavelength (CWL) is the arithmetic mean of the wavelengths at 50% of peak transmission. The full width at half maximum (FWHM) is the FWHM at 50% of peak transmission. The degree to which a filter prevents transmission of wavelengths beyond the pass-band is referred to as blocking. Blocking is expressed as the ratio of energy transmitted beyond the pass-band to energy transmitted within the pass-band.

The most prominent application of band-pass filters is to improve the SNR. A proper filter needs to increase the detection of the signal while reducing the detection of the background noise. When selecting a filter, the filter curve is matched to the corona spectrum and the spectral profile of the solar noise. These factors affect how efficiently the signal is detected (Govire & Pete, 2007).

Correlation can also be considered as a type of numeric band pass filter and thus can be used as a technique for extracting a signal from noise (Tipton, 2000). Correlation compares two sequences to find out how similar they are. If the signals are identical they are said to have a correlation,  $R$  of unity. If they are completely different they don't correlate and  $R$  is zero.  $R$  is a dimensionless number and varies between 0-1 (Tipton, 2000).



## CHAPTER 3: METHODOLOGY

The first stage of the design process was to define the scope of the project and its boundaries. This involved an exploratory literature survey in the field of corona and Fraunhofer lines to arrive at an initial understanding of the problem statement. This included research into the current methods of corona detection and the plausibility of utilising the Fraunhofer lines as a method for detecting corona outside the solar blind region. Once the reference and research material was compiled it was necessary to define and clarify the research plan. Furthermore it was important to generate experimental tests to verify existing theory. The results generated from the experimental testing necessitated good design decisions for an optimal final outcome.

The following was the design approach taken during the research:

1. Define goal of study
2. Define scope
3. Define variables
4. Define data collection methods
5. Define measuring methods
6. Define analysis methods

The primary aim of the study was to investigate and understand whether the use of Fraunhofer lines was a possible method of detecting corona in the daylight. The possibility of a favourable outcome would allow for the potential production of a camera that was cheaper.

The type of research was exploratory and the research approach was of a quantitative nature where experimental tests were conducted to test hypotheses derived from theory and to explore certain concepts. After a thorough literature survey it was determined that the research question did have potential for further exploration.

The ideal approach was to consider the entire corona wavelength range however after defining the problem statement and realising that high resolution was required, the wavelength region of 338.67nm – 405nm was agreed upon. Experimental tests were conducted to test hypotheses derived from theory and to explore certain concepts. In addition experiments were conducted to obtain absolute data on corona since this was not available in existing literature and was of fundamental importance in investigating the research questions. All the experiments were conducted in the CSIR EO lab with a HV power supply and a point-sphere corona source. The primary variables were voltage, environmental parameters and the geometry of the corona source which contributed to the absolute intensity of the corona spectrum. The measurements were done using a Specline Avantes spectroradiometer and MATLAB software was used for the analysis of the results. The analysis method was to determine the SNR and thereafter optimize it through signal processing methods.

After performing the experiments to investigate the filter efficacy in segregating the corona signal from the solar background, it was concluded that the purchased optical filter was not capable of detecting the corona peak at 393.148nm. Consequently it was decided that possibly the optical filter specifications were not ideal so a new approach of simulating an optical narrow band - pass filter in MATLAB was executed to improve the SNR.

The FWHM of the filter and the CWL were adjusted and moved along the wavelength range evaluating the SNR at each wavelength and CWL. The maximum SNR was thereafter displayed together with the wavelength and FWHM of the filter. This new approach was intended to generate an ideal filter with an ideal CWL and FWHM.

## CHAPTER 4: EQUIPMENT USED AND EXPERIMENTAL RESULTS

The following chapter will describe the equipment used for the experiments together with the experimental and signal processing results. In addition an in-depth discussion of the results achieved is included.

### 4.1 Equipment used

Starline AvaSpec 2048L spectrometer (Jorgie, 2013)

*Wavelength Range:* 338.67 nm – 405 nm

The wavelength range is a key parameter that defines the appropriate diffraction grating choice. The higher line density diffraction grating (lines/mm) provides higher resolution which was required for the experiments. UV and visible light were the regions of the solar spectrum investigated.

*Detector choice:* The Starline AvaSpec is better for UV detection than standard CCD detectors.

*Optical resolution and slit size:* Since higher resolution was required for the narrow Fraunhofer lines a 2400 lines/mm diffraction grating was selected. This has the effect of limiting the instrument to a more narrow range. For the best resolution a small slit width was used.

Slit width is a key factor in determining both resolution and throughput into the optical bench. There was also a replaceable slit kit that made the spectrometer a versatile instrument for both high resolution and low sensitivity measurements or high sensitivity and low resolution measurements.

Table 4 shows the optical resolution for each of the slit widths in the slit kit.

Table 4: Slit width vs optical resolution

Slit Width( $\mu\text{m}$ )	Optical Resolution
25 $\mu\text{m}$	0.1537nm
50 $\mu\text{m}$	0.2379nm
100 $\mu\text{m}$	0.4392nm
200 $\mu\text{m}$	0.8789nm

NB: The highlighted portion in Table 4 was the selected slit width for the experiments .

*Sensitivity:* Since a high photometric sensitivity was required due to the corona signal intensity being so low, a high throughput optical bench and a high quantum efficient detector were selected. In addition a detector lens was obtained which focused light from the larger core optic fibre onto the smaller detector pixels.

*Grating* (VE 340-640 $\pm$ 70nm is the spectral range): The spectral range depends on the starting wavelength of the diffraction grating. The larger the wavelength the smaller the range. The diffraction grating determines how far the different wavelengths are separated (dispersed) at the detector array. Additionally the optic fibre core diameter affects the width of the light beam and thus is an important parameter in resolution.

Resolution (line pairs/mm) is defined as follows:

$$r = \frac{1}{2D} \quad (17)$$

- where D is the diameter of the optic fibre core in mm.

Figure 29 shows the inverse relationship between fibre diameter and resolution.

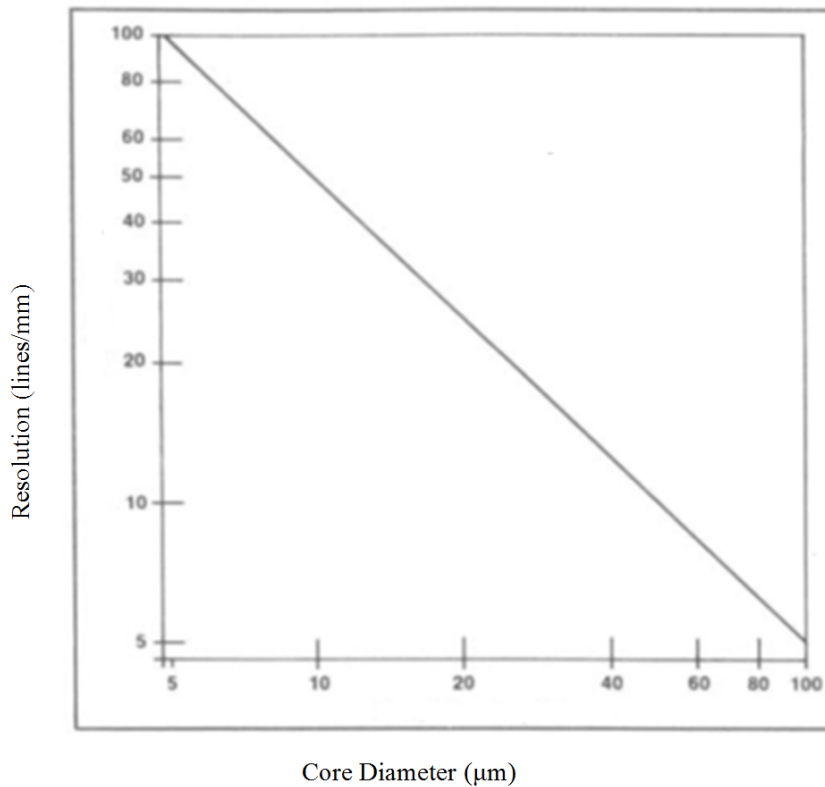


Figure 29: Relationship between fibre diameter and resolution (Wako, 2011)

The resolution of the optic fibre used was 1.25 line pairs/mm where  $D=0.4\text{mm}$ . The CCD detector had a large number of pixels, high sensitivity and high speed. More pixels provide a higher resolution or a larger FWHM.

Band Pass Filter (Materion, 2013)

Table 5: Specifications of the optical band-pass filter

FWHM	0.3nm
CWL	393.37nm
Diameter	1 inch
$\%T_{\lambda}$	67%
OD	0.174

The FWHM chosen was to ensure the lowest point of the Fraunhofer line was observable. In addition the intensity of the Fraunhofer line at 393.68nm was much lower when compared with the other Fraunhofer lines. This provided a better SNR in relation to the other Fraunhofer lines. Furthermore the corona peak at 393.140nm fell within the FWHM of the filter.

### Cosine Corrector: 5° aperture

The irradiance or illuminance falling on any surface varies with the cosine of the incident angle as shown in Figure 30.

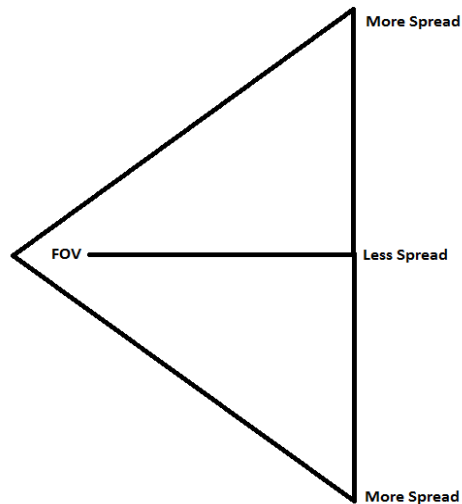


Figure 30: Schematic describing operation of the cosine corrector

A cosine corrector is used to correct the spatial responsivity. (Jorgie, 2013). Figure 31 is an image of the cosine corrector used in the experiments.



Figure 31: Cosine corrector (Jorgie, 2013)

### Corona Source - Point-Sphere Configuration

Corona discharges on high voltage conductors occur at points with the highest electrical stress. Conductors that consist of sharp points, or spheres with small radii, are more prone to causing corona (due to the higher electric field) (Loeb, 1939). Figure 32 is the point-sphere corona source used in the experimental testing.

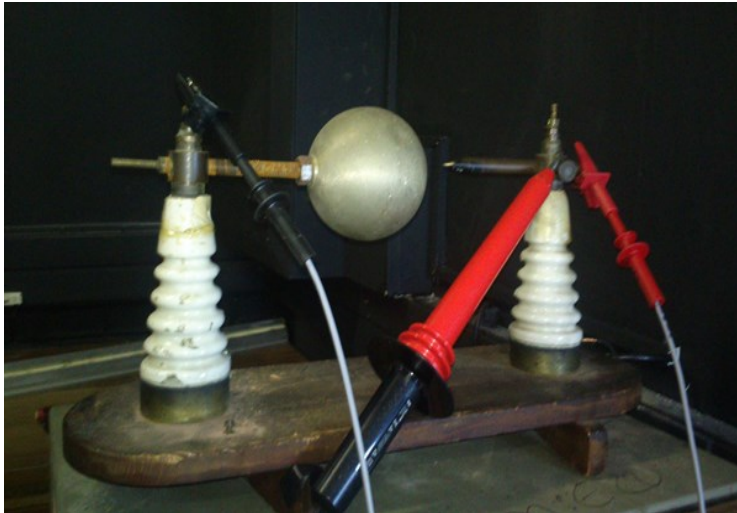


Figure 32: Point-sphere corona source

### Biconvex lens

A collimated beam of light passing through the biconvex lens is converged (or focused) to a spot behind the lens. The biconvex lens ensures maximum light enters the optic fibre (Khurana, 2008). This is represented in Figure 33.

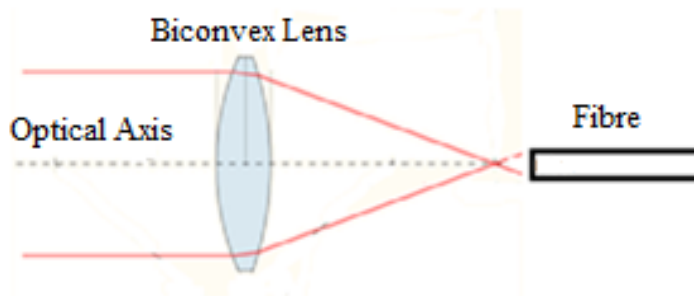


Figure 33: Converging Lens

### Cassegrain

The Cassegrain has a parabolic primary mirror and a hyperbolic secondary mirror that reflects the light back down through a hole in the primary mirror. The parabolic mirror reflects parallel light rays entering the telescope to its focus, which is also the focus of the hyperbolic mirror. The hyperbolic mirror then reflects those light rays to its other focus, where the image is observed.



Figure 34: Cassegrain (SC, 2001)

## Hipotronics Power Supply (AC/DC)

Figure 35 is the power supply used in the experimental testing.



Figure 35: Hipotronics power supply

## 4.2 Experimental and Signal Processing Results

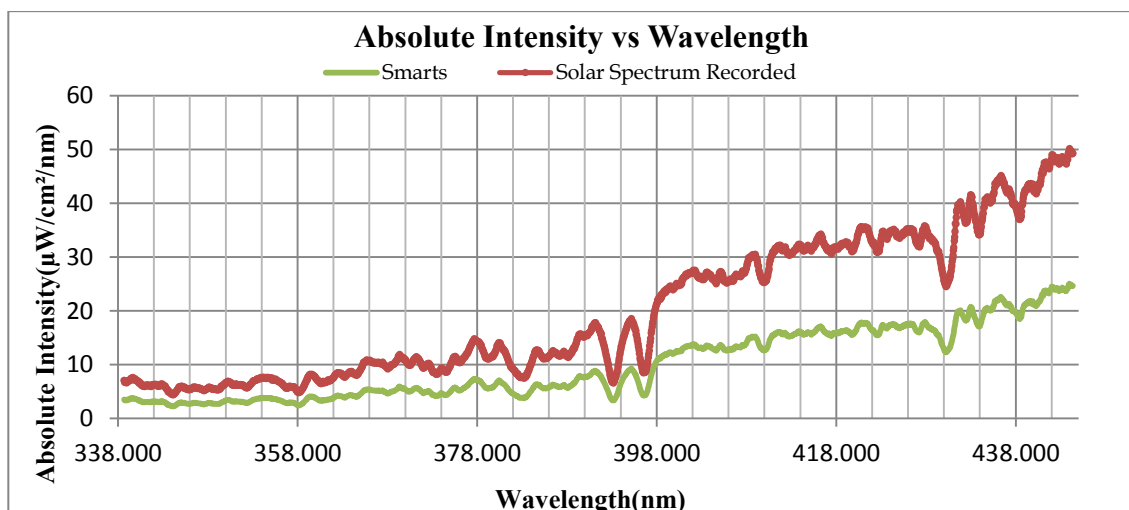
### 4.2.1 Measurement of the solar spectrum in absolute units and comparison with the model obtained from SMARTS

The equipment used was:

- Avantes Starline spectroradiometer AvaSpec-2048L
- Dell Laptop with Avasoft8

Methodology:

The fibre probe was pointed towards the sun and the spectrum was recorded using Avasoft8. The results are shown in Graph 1.



Graph 1: Solar spectrum recorded and solar spectrum from SMARTSs

It is evident that the shapes of the spectra are identical. The intensity varies between the SMARTS and the recorded spectra since some of the parameters required in SMARTS were taken as the default values since it was not possible to measure these parameters due to the absence of the appropriate measuring equipment.

#### 4.2.2 Determination of the transmission curve of the cosine corrector

The aim was to calibrate the cosine corrector and obtain the transmission curve of the cosine corrector. This was to obtain absolute measurements of low intensity corona without the use of the corrector.

The equipment used was:

- Avantes Starline spectradiometer AvaSpec-2048L
- Cosine Corrector-5° aperture ( cosine corrector accepts light at 5° field of view)
- Dell laptop

The methodology was to record the solar spectrum with the cosine corrector and thereafter record the solar spectrum without the cosine corrector using a 200μm slit width for a high throughput. This is shown in Graph 2. The cosine corrector transmission curve shown in Graph 3 is the ratio of the solar spectrum with the cosine corrector and the solar spectrum without the cosine corrector. The experimental setup is shown in Figure 36.

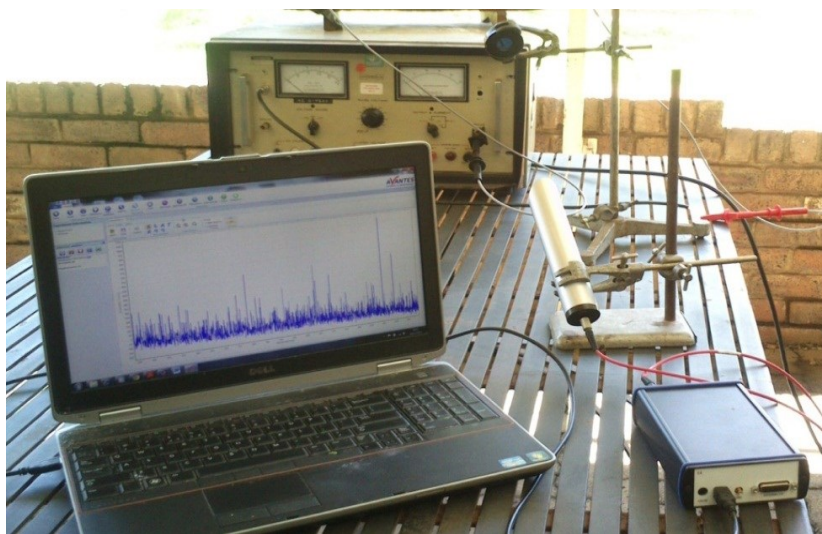
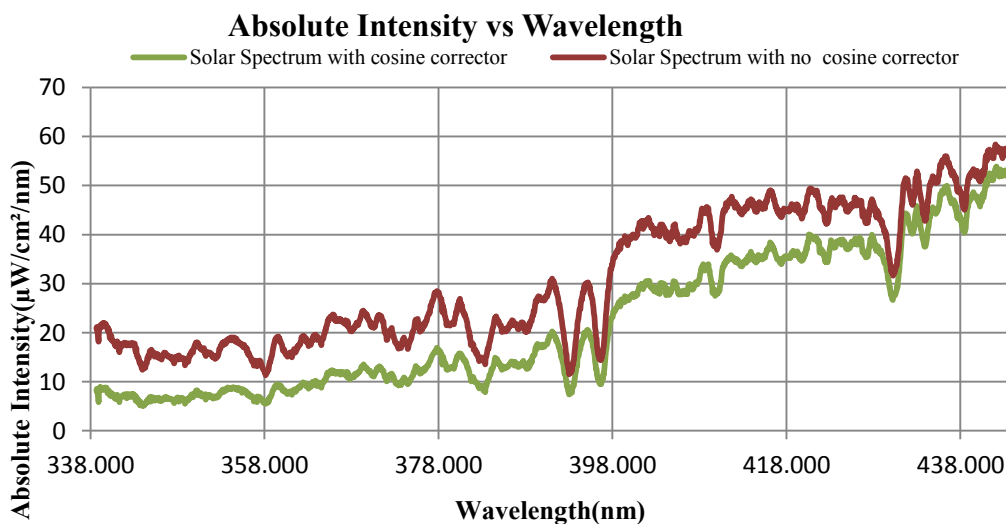
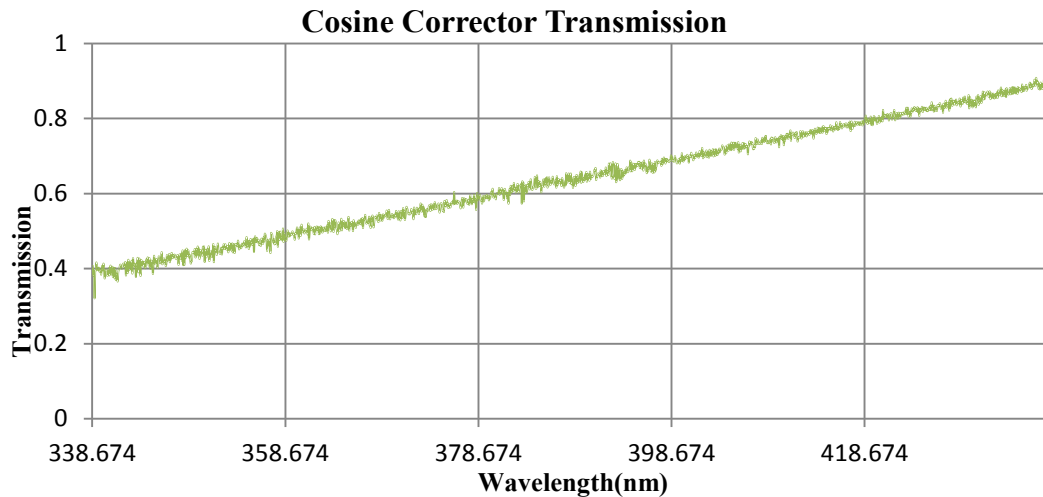


Figure 36: Experimental setup

#### Results:



Graph 2: Solar spectrum with and without cosine corrector



Graph 3: Calculated cosine corrector transmission curve

One of the factors contributing to the overall uncertainty of spectral measurements is the cosine error of the spectroradiometer. It leads to measurement errors that depend on atmospheric conditions and on the solar zenith angle and the time of day and the season. A closer examination of both spectra shows that the intensity is less with cosine correction. Cosine correctors eliminate the optical interface problems associated with light collection. A cosine corrector corrects for the light entering the meter at angles other than 90°.

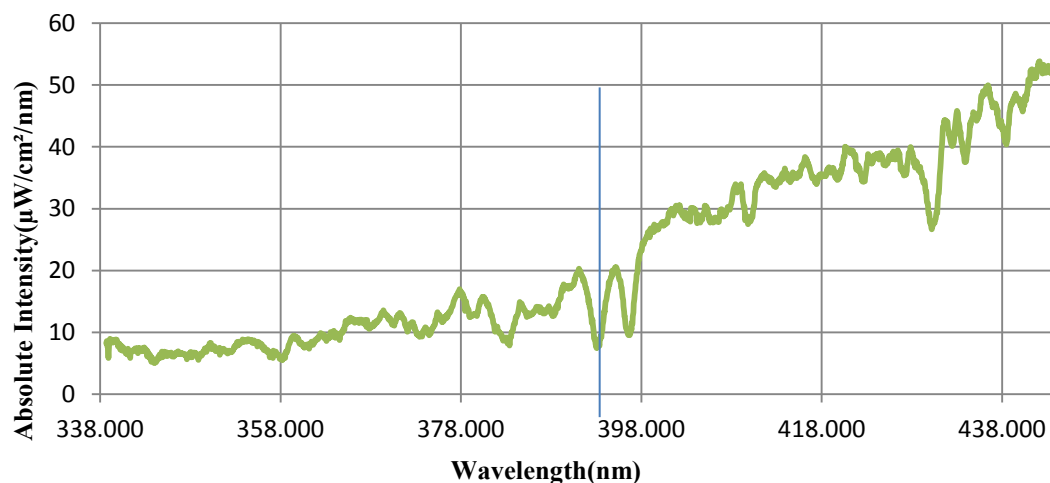
#### 4.2.3 Verifying the Element at 393.682nm in the solar spectrum

The aim was to determine and verify that the Fraunhofer line at 393.682nm is due to the element Ca<sup>2+</sup>.

The equipment used was the Dell laptop with Plasus SpecLine software installed and a previously recorded solar spectrum. The solar spectrum was loaded into the Plasus SpecLine software and the element responsible for the Fraunhofer line at 393.682nm was determined.

#### Results:

#### Absolute Intensity vs Wavelength



Graph 4: Solar spectrum indicating Ca II at 393.3682nm(blue line in graph)

The theory was validated by the Plasus Specline software.



#### 4.2.4 Experimental setup and the implementation of the lens and alignment method for all corona spectrum recordings

The aim was to ensure maximum throughput into the optic fiber which served as the basis for all other corona experiments performed.

The equipment used was:

- Hipotronics power supply
- Corona source : point-sphere configuration
- Convex lens
- Class 3 laser: max output <math><5\text{mW}</math>, wavelength range: - Avantes Starline spectrometer AvaSpec-2048L
- Dell laptop
- $200\mu\text{m}$  slit width – for high throughput
- Paper attached to tip of point–sphere gap geometry

The laser was shone backwards through the optic fibre probe and the lens was adjusted to ensure the laser diffracts out into a cone of light. Thereafter the corona tip position was adjusted i.e. either backwards, forwards, up or down until a round small red dot was observed on the paper attached to the tip of the point. The experimental setup is shown in Figure 37 and Figure 38.

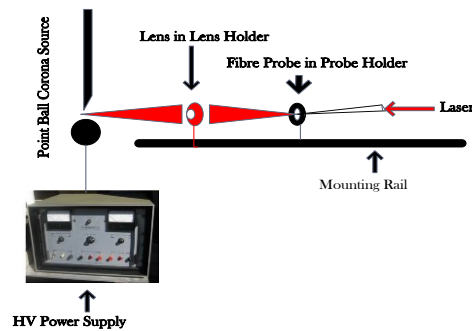


Figure 37: Schematic of lens alignment process

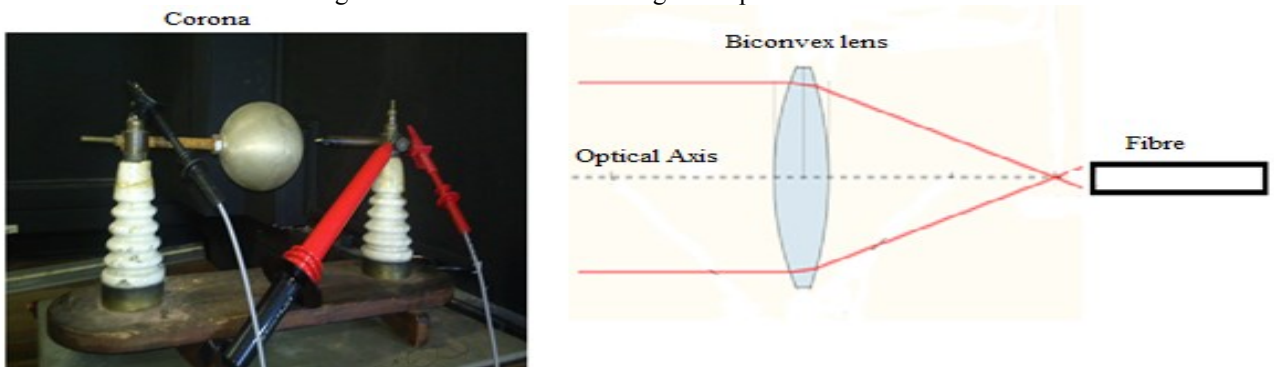


Figure 38: Application of lens alignment setup

This alignment setup ensures that the corona point source is directly focussed on the probe to ensure maximum throughput into the optic fiber.

#### 4.2.5 Verification of the corona inception voltage and the visible corona inception voltage

The aim was to validate the theory.

The equipment used was:

- Hipotronics power supply
- Corona source : point-sphere gap geometry
- Ruler to measure the distance between the tip and the sphere
- Weather meter to measure temperature
- Venier calliper to measure the diameter of the corona tip

The methodology was:

- Record the temperature and the pressure.
- Measure the distance between the tip and the sphere.
- Measure the diameter of the tip.
- Record the corona inception voltage and the visible corona inception voltage.

The experimental setup is shown in Figure 39.



Figure 39: Experimental setup

#### Results:

- $T=19.5^{\circ}\text{C}$
- $p=1025\text{millibars}$  or  $76.8813\text{cmHg}$
- $r=0.0052\text{cm}$
- $d=0.11\text{cm}$
- $m=m_v=0.93$
- $\delta=1.03$

Table 6: Calculated and measured voltages

Voltage(V)	Calculated	Measured
Corona inception voltage	$V_D = 3.37 \text{ kV}_{\text{rms}}$	$V_D = 5.4 \text{ kV}_{\text{rms}}$
Visible corona inception voltage	$V_V = 7.835 \text{ kV}_{\text{rms}}$	$V_V = 7 \text{ kV}_{\text{rms}}$

Using the formula for percentage error:

$$E = \frac{\text{Measured} - \text{Calculated}}{\text{Calculated}} \times 100 \quad (18)$$

The error was determined for both the corona inception voltage and visible corona inception voltage.

Corona inception voltage error:  $E_D=61\%$

Visible corona inception voltage error:  $E_V=10.68\%$

The above errors are mainly attributed to instrument errors, weathering of the corona-point sphere configuration i.e. in m estimation, and operator errors(ears and eyes). Instruments often have both systematic and random errors.

#### 4.2.6 Investigation of the effect of varying DC voltage on the corona spectrum

The aim was to determine whether the Stark effect i.e. shifts and broadening of the corona spectra is prevalent and the effect on absolute intensity. It was important to determine whether possibly the corona CWL would shift outside the filter pass-band in order to determine if the optical filter worked for different voltages.

The equipment used was:

- Hipotronics power supply (DC)
- Corona source – point-sphere gap geometry with a paper attached to tip of point for alignment purposes
- Convex lens , Class 3 laser: max output <5mW, wavelength range: 650nm±10nm
- Avantes Starline spectrometer Avaspec-2048L
- Dell laptop
- 200µm slit width – for high throughput
- Distance between rod and sphere = 6mm

The methodology was:

- Align the fibre probe to ensure maximum throughput into the meter.
- Increase the voltage from and record the spectra.
- Set integration time of spectroradiometer to 2 sec to ensure a high sensitivity.

The experimental setup is shown in Figure 40 and Figure 41.

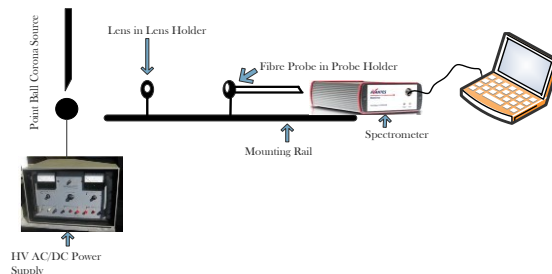


Figure 40: Schematic of experimental setup

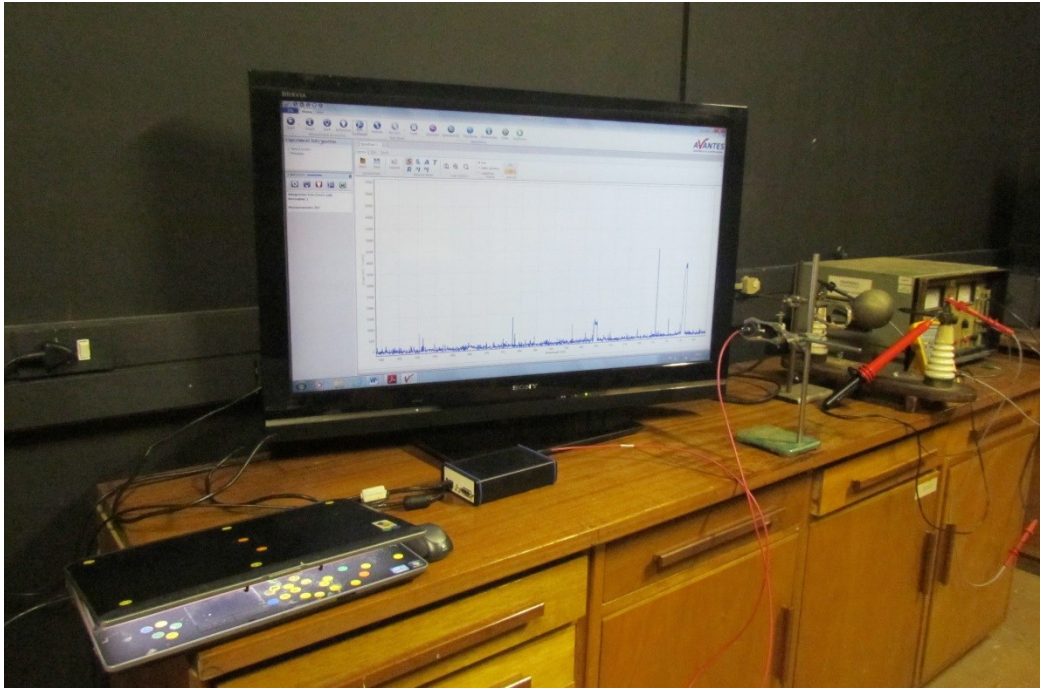
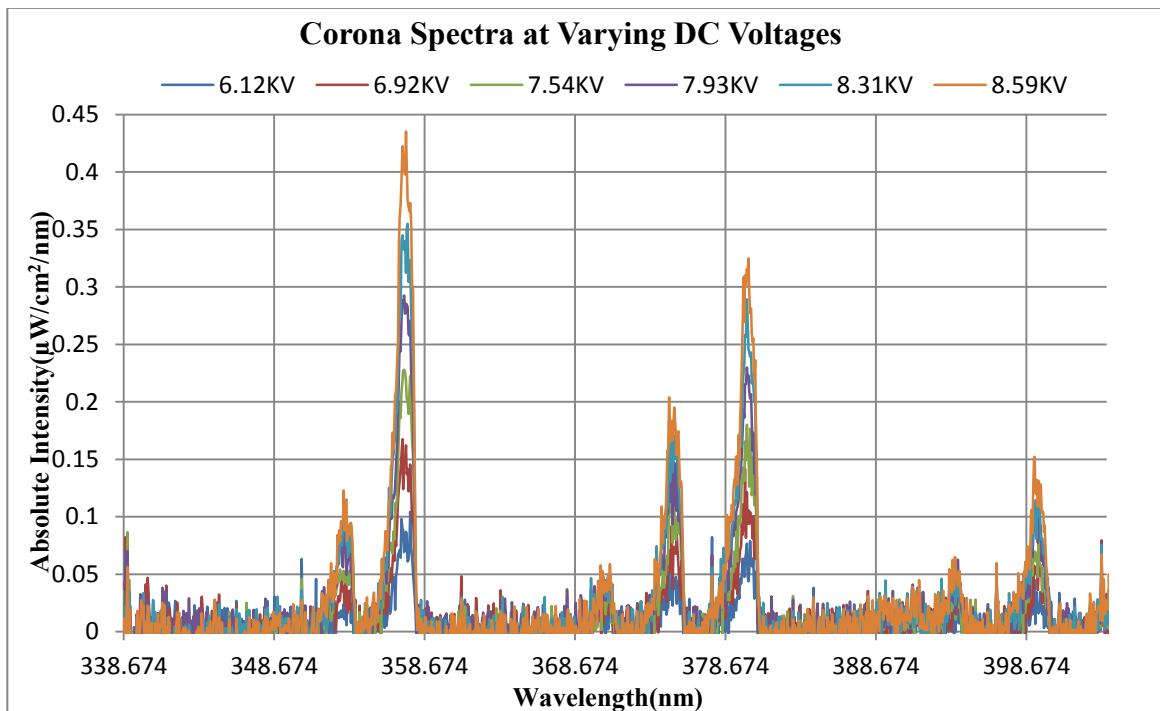


Figure 41: Photograph of experimental setup

**Results:**



Graph 5: Recorded corona spectra at varying DC Voltage

From the recorded spectra no changes in the spectral line width, spectral profile and CWL were observed contrary to existing literature. At voltages < 30kV there is no concern for corona peak shifting out of the filter pass-band. More experiments need to be conducted at higher voltages.

#### 4.2.7 Investigation of Positive and Negative corona

The aim was to determine whether there exists a difference in the spectrum of positive corona and negative corona. It is important to determine whether the corona CWL would move outside the optical filter pass- band.

The equipment used was:

- Hipotronics power supply (DC)
- Corona source – point-sphere gap geometry with a paper attached to tip of point for alignment purposes
- Convex lens
- Class 3 laser: max output, wavelength range:  $650\text{nm} \pm 10\text{nm}$
- Avantes Starline spectrometer AvaSpec-2048L
- Dell laptop
- $200\mu\text{m}$  slit width – for high throughput
- Distance between rod and sphere = 6mm

The methodology was:

- Align the fibre probe to ensure maximum throughput into the meter.
- Adjust the polarity of the supply voltage to generate positive and negative corona.
- The voltage was set to 7.12KV for positive corona and -7.12KV for negative corona
- Integration time of spectroradiometer: 2sec for high signal sensitivity.

The experimental setup is shown in Figure 42

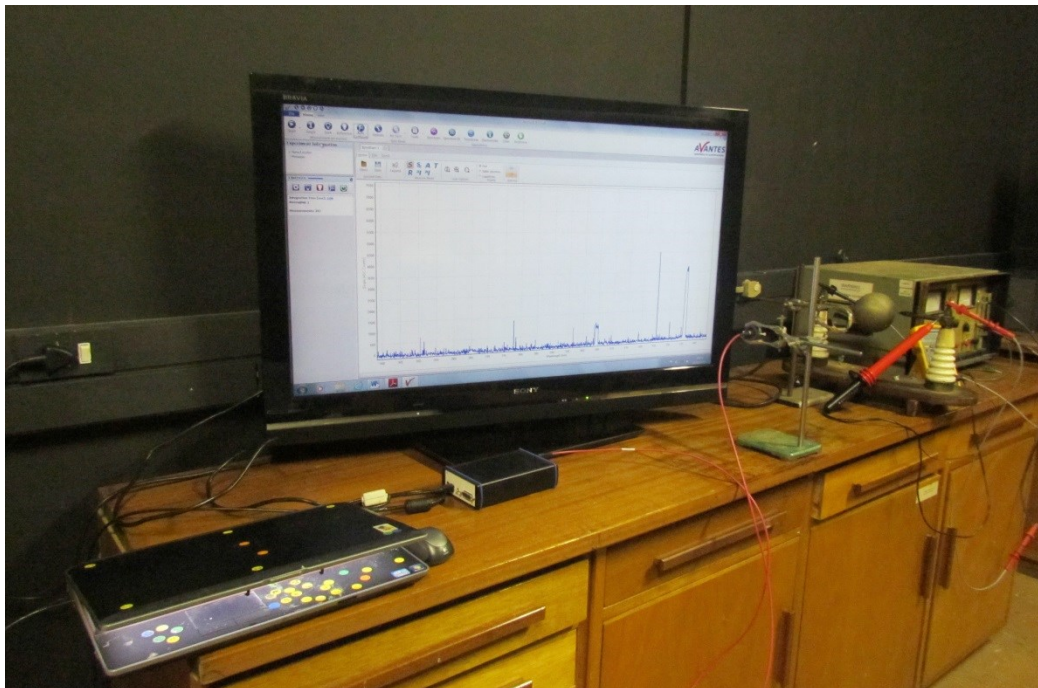
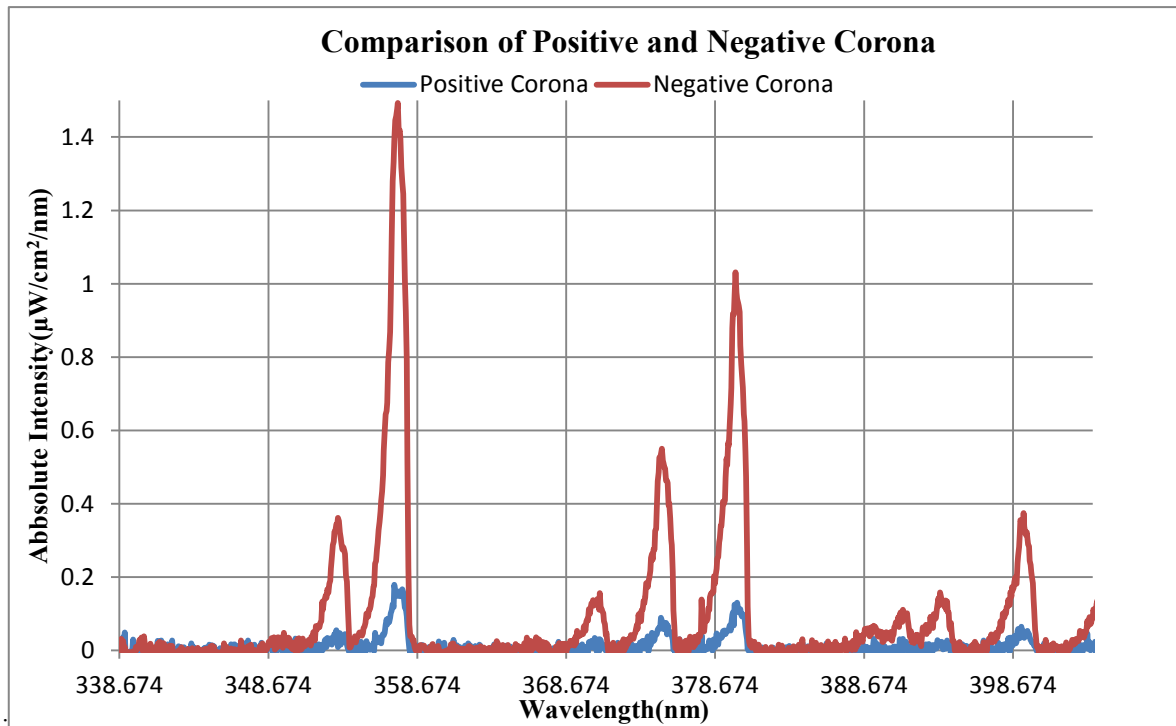


Figure 42: Experimental Setup

## Results:



Graph 6: Recorded positive and negative corona spectra

It was noted that there was an increase in intensity for negative corona as described in the literature. In addition there was no peak shifting between positive and negative corona which was important since corona CWL shifting would move the corona peak outside the optical filter pass-band.

### 4.2.8 Verification of the optical band-pass filter response in the ambient environment

The aim was to confirm the specifications of the optical band-pass filter i.e. the absorption and transmission curves and to investigate the effect of filter orientation on CWL and transmission.

The equipment used was:

- 0.3nm optical band-pass filter , CWL= 393nm
- Solar signal - sun
- Avantes Starline spectrometer AvaSpec-2048L
- Dell laptop
- 200µm slit width – for high throughput

The setup was aligned outside with the narrow band- pass optical filter. The probe was directed toward the sun with the filter in place and a spectrum was recorded. Thereafter the solar spectrum was recorded without the filter. The transmission curve was evaluated by dividing the filtered solar spectrum by the solar spectrum with the filter. The absorption was evaluated by the following equation:

$$\text{Absorbtion}=1-\text{Transmission} \quad (19)$$

The experimental setup is shown in Figure 43 and Figure 44.

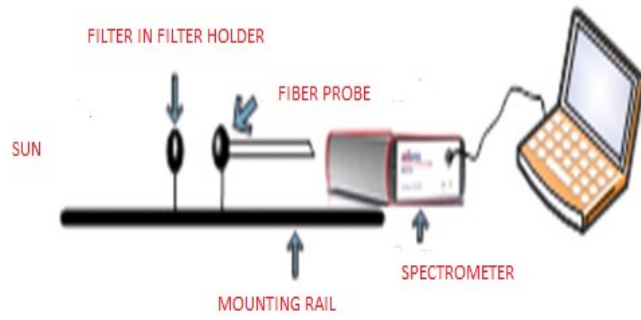


Figure 43: Experimental setup

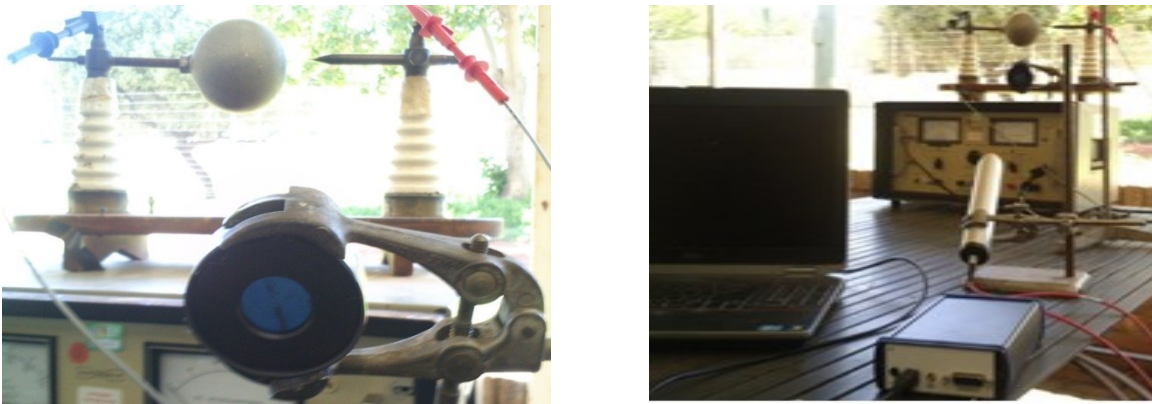
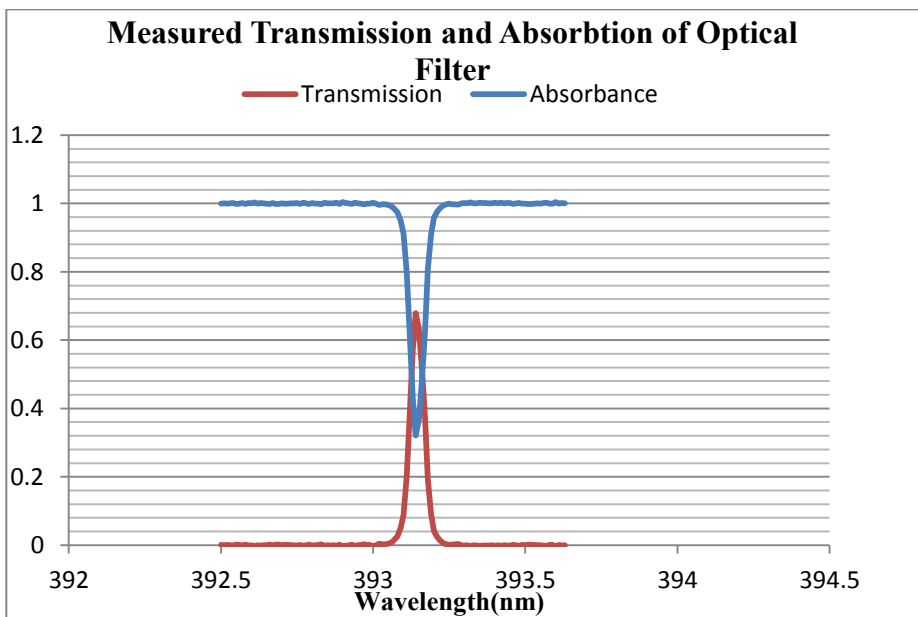
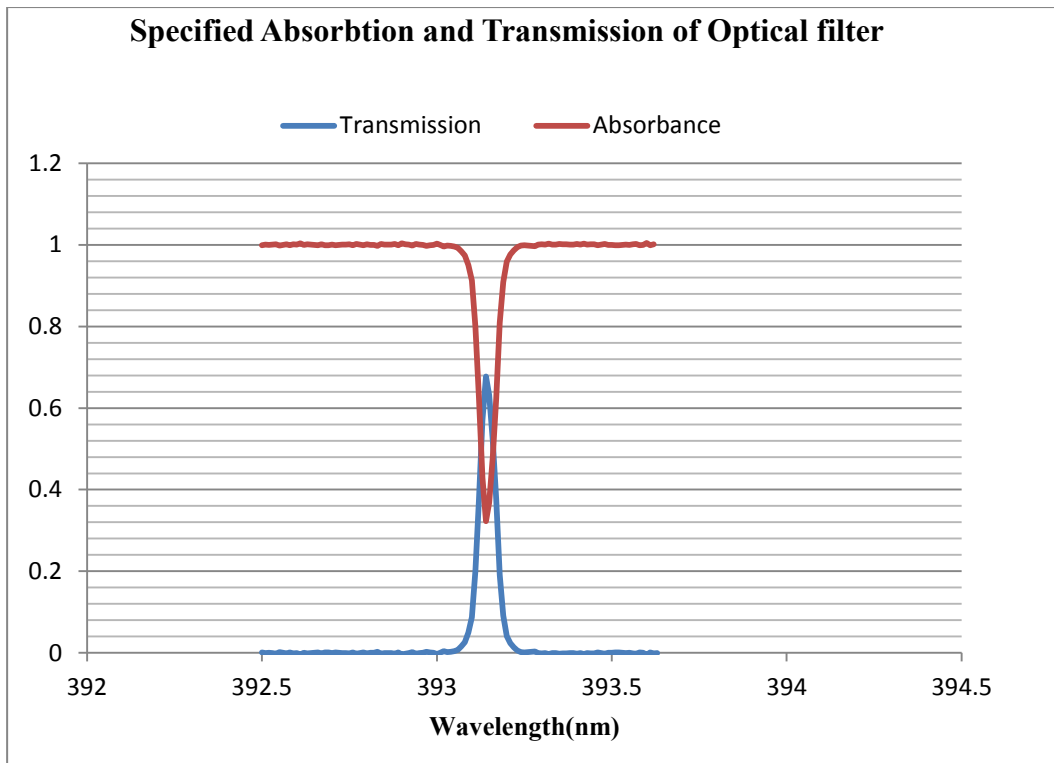


Figure 44: Photograph of Experimental setup

**Results:**



Graph 7: Measured absorption and transmission of the optical filter



Graph 8: Specified transmission and absorption of the optical band-pass filter

Using the formula:  $E = \frac{(\text{Peak transmission} - \text{Specified transmission})}{\text{Specified transmission}} \times 100\%$ ,  $E = 0.2\%$ . The error is minimal and attributed to instrument and operator errors.

#### 4.2.9 Practical Implementation of the optical band-pass filter in a Cassagrain

The aim was to investigate the filter efficacy in segregating the corona signal from the solar background noise.

The equipment used was:

- Cassagrain
- Avantes Starline spectrometer AvaSpec-2048L
- 200 $\mu\text{m}$  slit – for high throughput
- Dell laptop
- 0.3nm optical band pass filter , CWL=393nm
- Corona source - point-sphere gap geometry
- Hipotronics HV power supply

The methodology was:

The cassagrain with optical filter and probe were aligned with the corona source. This was done with the filter removed followed by shining the laser on the tip of the corona source (to ensure proper alignment and maximum throughput) and thereafter careful insertion (to avoid misalignment and concerns to the throughput) of the filter back in the cassagrain. The voltage was initially set to the corona inception voltage of 5.4kV. It was ideally expected that the optical filter would remove the solar noise and the remaining signal recorded would be corona. Furthermore the signal-to-noise ratio of the output signal would be higher when compared to the non-filtered input signal.



The experimental setup is shown in Figure 45.



Figure 45: Experimental setup

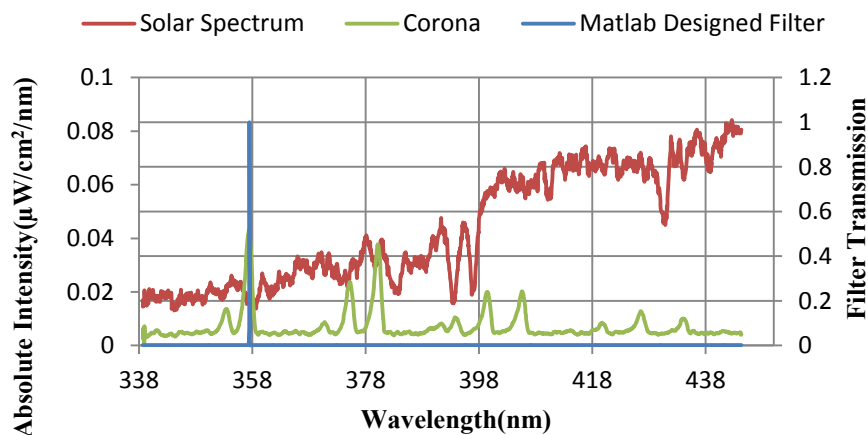
Firstly there was no corona detected at the corona inception voltage. Thereafter the voltage was increased and still no corona was observed. After much discussions and research, it was decided that the filter specifications i.e. the FWHM and CWL were not correct. Since the expected ideal was not achieved a new approach of mathematically designing and simulating a filter with the suitable FWHM and CWL was executed to improve the signal-to-noise ratio.

#### 4.2.10 Filter Design

The aim was to design an optical band-pass filter which swept along the entire wavelength range 338.672nm – 405nm until the highest SNR was obtained. Software was written in MATLAB to generate a shape-controllable narrowband optical band-pass filter which moved along the entire wavelength range 338.674nm – 405nm. The solar and corona spectra used in the code were measured using the spectroradiometer and the filter transmission curve used was the curve obtained from experimental tests. The FWHM and CWL of the filter were altered until the highest SNR was obtained. Various combinations of FWHM intervals were chosen and tested until the optimal FWHM and CWL were achieved.

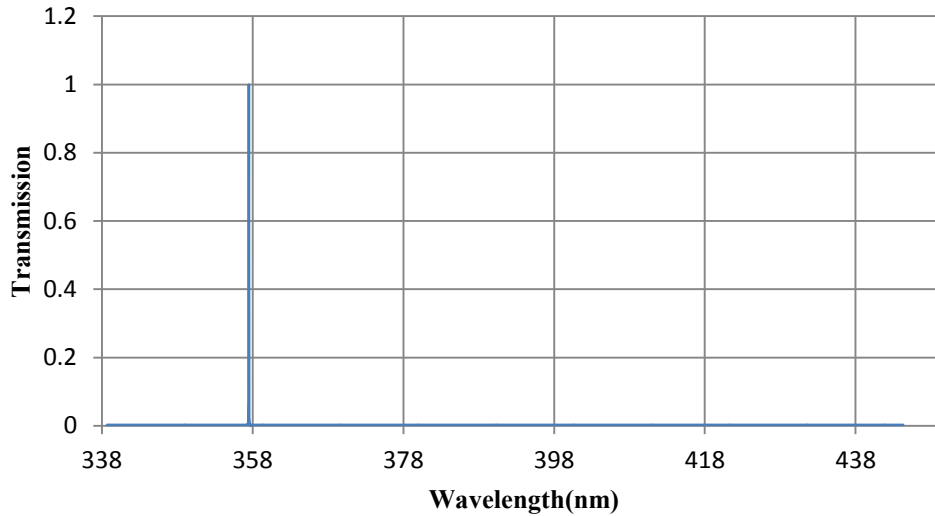
#### Results:

#### Graphs of MATLAB Results



Graph 9: MATLAB generated transmission curve of the filter and corona and solar spectra

### Transmission Curve of MATLAB Designed Narrow Band - Pass Filter



Graph 10: Ideal filter transmission

Table 7: Results

Tests	FWHM(nm)	CWL(nm)	SNR
Filtered signal using MATLAB simulated filter.	0.05	357.558	2.121
Filtered signal using purchased optical filter.	0.3	357.455	0.00314
Filtered signal using purchased optical filter at selected Fraunhofer line	0.3	393.37	0.0026

From Table 7 it is evident that filter design is fundamental in improving the SNR. Filtered results showed the improvement of the SNR when compared with unfiltered results. In addition the newly designed band-pass filter generated a much higher SNR when compared with the old filter with a FWHM of 0.3nm. The results verified that with the newly designed filter the signal to noise ratio increased by 67%

#### 4.2.11 Cross correlation Processing

The aim was to investigate cross correlation as a potential method to detect corona. Cross correlation was performed with different solar spectra, a corona spectrum and a noise threshold. The Pearson coefficient was determined and analysed. The noise was generated in Excel using the rand function.

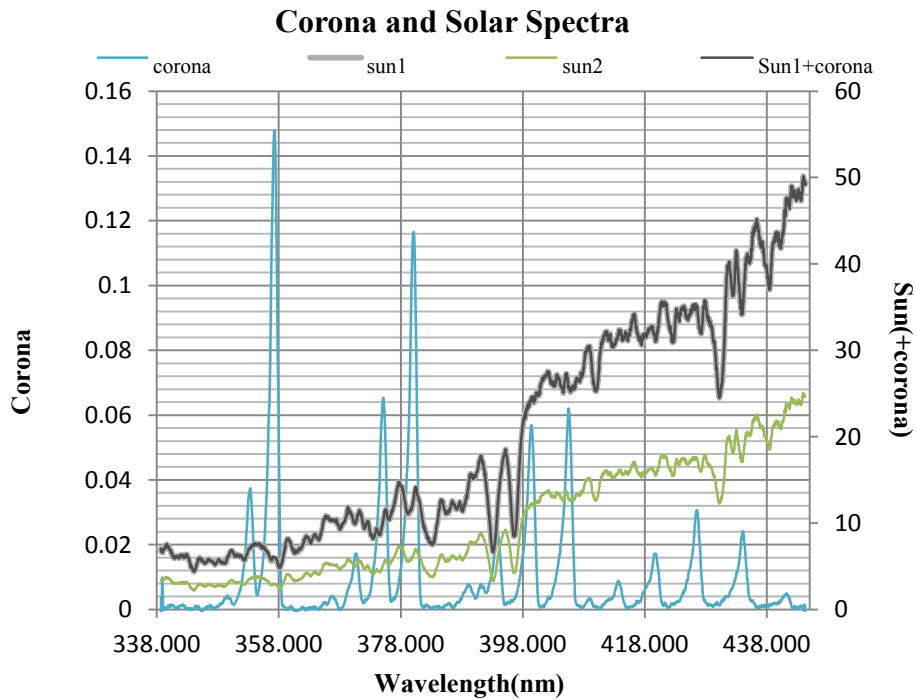
**Results:** The results of cross correlation are shown in Table 8.

Table 8: Correlation results

<b>c* sun1</b>	False
<b>c*sun2</b>	False
<b>c* (sun1+noise)</b>	False
<b>c* (sun2+noise)</b>	False
<b>c* (sun1+corona)</b>	True
<b>c* (sun2+corona)</b>	True
<b>c* (sun1+noise+corona)</b>	True
<b>c* (sun2+noise+corona)</b>	True

NB:

- \* is correlation.
- c is the corona spectrum.
- sun1 is when the solar spectrum was recorded under intense sunlight.
- sun2 is when the spectrum was recorded under cloudy conditions.



Graph 11: Corona and solar spectra

**NB:** sun1 graph overlaps sun1+corona

It was noted that when the corona template was correlated with different solar spectra recorded at different times of the day with different intensities, the same correlation coefficient resulted. Thereafter the corona spectra template was correlated with the solar + corona spectra. This resulted in different coefficients which was indicative that corona was present. To create a more realistic approach, noise was included with the corona + solar spectra and correlated with the corona template and different correlation coefficients were generated.

In essence the results of cross correlation indicated that corona was present when the corona template was correlated with the solar+corona spectrum. This result of the experiment indicates that this could be a prospective new method of detecting corona.

## CHAPTER 5: CONCLUSIONS AND RECOMMENDATIONS FOR FURTHER WORK

### 5.1 Conclusions

This dissertation has investigated Fraunhofer lines in the solar spectrum as a method to detect corona. The hypothesis was that there is an overlap between certain Fraunhofer lines and corona emission peaks which could conceivably be exploited as a way of detecting corona during daylight. The wavelength range 338.67nm – 405nm was the selected range since there existed many corona peaks which are of a considerably higher intensity. The Fraunhofer line at a wavelength of 393.13682nm and the corona peak at 393.148nm were chosen for the experiments. An optical band-pass filter with a central wavelength of 393.37nm with a FWHM of 0.3nm was used for filtering of the signal. After performing the experiments and evaluating the results it was determined that the SNR had not improved. The signal to noise ratio was 0.0314. Consequently it was decided that the optical filter specifications (i.e. FWHM and CWL) were not ideal. Hence a new approach of simulating an optical narrow band-pass filter in MATLAB was designed that swept along the the wavelength range evaluating the SNR to generate the ideal filter. The filter specifications that generated the highest SNR had a FWHM of 0.05nm and a CWL of 357.558nm which coincided with the wavelength of a different Fraunhofer line. The signal to noise ratio was 2.121. The results verified that with the newly designed filter the signal to noise ratio increased by 67%. In essence Fraunhofer lines can be used to detect corona activity during the daytime with the implementation of a suitable filter

Thereafter cross correlation was investigated and this proved to be an extremely encouraging and promising area for corona detection. The results of the cross correlation indicated that corona was present when the corona template was correlated with the solar+corona spectrum.

The research questions were:

1. Is there a correlation between the measured and published corona and solar spectra?

After performing experiments and researching spectra in the literature it was concluded that published and measured spectra were comparable in terms of shape and relative intensity. Recorded solar spectra using a spectroradiometer were compared with the reference spectra generated from the SMARTS package. The comparison revealed that the shape profiles of the reference and measured spectra were similar. In addition published corona spectra for varying voltages were compared with the spectra recorded. The published and recorded corona spectra were similar in shape.

2. Do the wavelength and intensity of the corona peaks vary under applied voltage?

The effect of both positive and negative polarity on the corona spectrum was reviewed. It was noted that there was an increase in intensity for negative corona as verified in the literature. Furthermore there was no peak shifting between positive and negative corona. Subsequently the effect of varying voltage on the corona spectra was investigated. The results showed that as the supply voltage increased the intensity of the corona peaks increased. Additionally at voltages < 30kV there was no corona peak shifting. However since the range of the power supply was limited, there was no way to see the effects at higher voltages (Loeb, 1939). In existing literature (Loeb, 1939) Lawrence and Dunnington observed peak shifting of the corona spectra (Stark effect) at high electric fields.

3. Can signal processing improve the SNR?

The signal processing techniques employed to answer this question involved simulating a band-pass filter with an adjustable FWHM that moved along the wavelength range until the highest signal-to-noise ratio was achieved. The newly designed filter of FWHM 0.05nm generated the highest SNR of 2.121 at a CWL of 357.558nm. The results verify that the SNR was higher with the new filter.

Thereafter cross correlation was performed. This method was able to detect corona in the presence of solar radiation. Hence signal processing can improve the SNR.

#### 4. Can the Fraunhofer lines be used to detect corona in the wavelength range 338.67nm – 405nm?

It was concluded that the particular Fraunhofer line selected (393.37nm) cannot be used for corona detection in daylight. However corona was detected at a different Fraunhofer line (357,558nm) . Hence Fraunhofer lines can be used to detect corona in an effective manner through the implementation of an extremely narrow optical band - pass filter and intelligent signal processing .

The thesis has resulted in recommendations for future work in corona detection methods.

#### 5.2 Recommendations for further work

- Cross correlation has potential and is an area where more research and future work should be done.
- If possible, an optical filter with the specifications generated in the MATLAB model should be purchased and the previous experiments repeated.

## REFERENCES

- Averill, B. A. a. E. P., 2007. *General Chemistry: Principles, Patterns, and Applications, v. 1.0 (2 Volume Set)*. s.l.:s.n.
- Averill, B. A. & Eldredge, P., 2007. *General Chemistry: Principles, Patterns, and Applications*. s.l.:s.n.
- Bird, R., Hulstrom, R. & Lewis, L., 1983. Terrestrial solar spectral data sets. *Solar Energy*, Volume Vol 30,, p. p 563..
- Bouchacourt, M. et al., 2003. Glow discharge optical emission spectrometry: moving towards reliable thin film analysis. *Analytical Atomic Spectrometry*, Issue 6.
- Chen, S., 1998. *Light spectra on AC Corona*. Japan, s.n.
- Czech, T., Sobczyk, A. T. & Jaworek, A., 2011. Optical emission spectroscopy of point plane corona and back - corona discharges in air. *The European Physical Journal D*, D(65), pp. 459-474.
- Education, P., n.d. *Chapter 2 Light and matter. The inner workings of the cosmos*. [Online]  
Available at:  
[http://wps.prenhall.com/wps/media/objects/610/625137/Chaisson/CH.00.002/HTML/CH.00.002\\_FM.htm](http://wps.prenhall.com/wps/media/objects/610/625137/Chaisson/CH.00.002/HTML/CH.00.002_FM.htm)  
[Accessed March 2013].
- Goldman, M. & Sigmond, R. S., 1982. Corona and Insulation. *IEEE Transactions on Electrical Insulation*, E(2), pp. 1-17.
- Govire, J. & Pete, A., 2007. *Edmund Optics Worldwide: Inside Filter2*. [Online]  
Available at: [http://www.edmundoptics.com/techsupport/resource\\_center/downloads/wp-inside-filters.pdf](http://www.edmundoptics.com/techsupport/resource_center/downloads/wp-inside-filters.pdf)  
[Accessed October 2013].
- Haver, T. O., 1997. *A Pragmatic Introduction to Signal Processing with applications in Chemical Analysis*, Maryland: s.n.
- Javadi, H., Farzaneh, M. & Peyda, A., 2010. Determination of electric field at inception based upon current -voltage characteristics of AC corona in rod - plane gaps. *Iranian Journal of Electrical and Electronic Enginnering*, 6(2).
- Johnson, D. H., 2006. *Scholarpedia*. [Online]  
Available at: [http://www.scholarpedia.org/article/Signal-to-noise\\_ratio](http://www.scholarpedia.org/article/Signal-to-noise_ratio)  
[Accessed September 2013].
- Jorgie, 2013. *Avantes*. [Online]  
Available at: <http://www.avantes.com/support/downloads>  
[Accessed March 2013].
- Khurana, A. K., 2008. *Theory and Practice of Optics and Refraction*. India: Elsevier.
- Kingsley, S. A., 1990. *Most Intense Fraunhofer lines*. [Online]  
Available at: [http://www.coseti.org/fraun\\_03.htm](http://www.coseti.org/fraun_03.htm)  
[Accessed March 2013].
- Loeb, L., 1939. *Fundamental Processes of electrical discharge in gases*. London: John Wiley & Sons.
- Loeb, L., 1965. *Electrical Coronas :Their Basic Physical Mechanisms*. California: University of California Press.
- Maruvada, S. P., 2000. *Corona Performance of High-Voltage Transmission Lines*. Baldock,Hertfordshire,England: Research Studies Press LTD.

- Maruvada, S. P., 2011. *Corona in transmission systems: Theory, design and performance*. South Africa: Crown Publications.
- Materion, 2013. *Filter Specifications*. s.l.:s.n.
- Michael A. Choma, M. V. S. C. Y. J. A. I., Sept 2003. Sensitivity advantage of swept source and Fourier domain optical coherence tomography. *Optics Express*, 18(11).
- Moore, P., Hickery, D. L. & Urbaneja, M., 2000. *Remote Sensing of Voltage Using Optical Assessment of Corona*. s.l., IEEE, pp. 1159-1164.
- Murphy, D. B. et al., 1999. *Optical Filters Information*. [Online]  
Available at: [http://www.globalspec.com/learnmore/optical\\_components\\_optics/optical\\_components/optical\\_filters](http://www.globalspec.com/learnmore/optical_components_optics/optical_components/optical_filters)  
[Accessed October 2013].
- Peek, F., 1929. *Dielectric Phenomena in High Voltage Engineering*. New York: McGraw-Hill Book Inc.
- R, J., 1987. *Sonar Beamforming and Signal Processing*. s.l.:Raytheon Co.
- SC, C. S.-C. t., 2001. *CGEM*. [Online]  
Available at: <http://www.astroshop.eu/celestron-schmidt-cassegrain-telescope-sc-280-2800-cgem-dx-1100-goto/p,25109>  
[Accessed October 2013].
- Schulze, P. et al., 2010. Gas chemical studies using corona discharge reactors. *The European Physical Journal*, D(60), pp. 637-644.
- Shimizu, K., 2011. Advanced air pollution. In: F. Nejadkoorki, ed. *Indoor air control by microplasma*. s.l.:s.n.
- Shixiu, S. Y. a. C., 1998. *Light Spectra on DC Corona*. Toyohashi, Japan, s.n.
- Singh, S., 2003. *Electric Power Generation: Transmission and Distribution*. s.l.:PHI.
- Tipton, R., 2000. All about Correlation. *Circuit Cellar*, Issue 17, pp. 58-62.
- Vosloo, W. L., Stolper, R. & Baker, P., 1997. Daylight Corona Discharge Observation and Recording system. *Proceedings of 10th International Symposium on HV Engineering*, Volume 6, pp. 161-164.
- Wako, A., 2011. *Echelle Spectrographs: Instruments covering a wide wavelength range with high spectral resolution*. [Online]  
Available at: <http://prc.nao.ac.jp/extra/uos/en/no02/>  
[Accessed March 2013].
- Walloston, W. H., 1802. A method of examining refractive and dispersive powers by prismatic refelction. *Philosophical Transactions of the Royal Society*, Issue 92, pp. 365-380.

## APPENDIX

Matlab code

<code>function NewSpectrum = SimFilter()</code>
<code>h=0;</code>
<code>%load('New_Data.mat');</code>
<code>load('New_Data2.mat');</code>
<code>PlotAll(Corona, Solar);</code>
<code>%initialising variables</code>
<code>snrMax = 0;</code>
<code>snr_no_filterinMax=0;</code>
<code>BestFilter = [0, 0, 0];</code>
<code>Best=[0 0 0];</code>
<code>snrMaxOld = 0;</code>
<code>BestFilterOld = [0, 0, 0];</code>
<code>%evaluating wavelength resolution</code>
<code>dl = Corona(2,1) - Corona(1,1);</code>
<code>%Evaluating width end such that filter lies within wavelength range after resampling</code>
<code>width_end=(342.440557617188-338.674000000000)/(dl*2048);</code>
<code>%Adjusting FWHM of filter</code>
<code>for width=[8:-0.1:width_end]</code>
<code>width</code>



<code>%generating new filter</code>
<code>NewFilter = resample(width, Filter);</code>
<code>max=0;</code>
<code>%finding the peak at a certain wavelength</code>
<code>for pos=1:length(Filter(:,1))</code>
<code>if (NewFilter(pos) &gt; max)</code>
<code>max = NewFilter(pos);</code>
<code>wavelength = pos;</code>
<code>end</code>
<code>end</code>
<code>%shifting filter</code>
<code>for n=1:length(NewFilter(:))</code>
<code>ShiftedFilter = circshift(NewFilter, n-wavelength);</code>
<code>%FWHM in nm</code>
<code>FilterWidth = length(ShiftedFilter(abs(ShiftedFilter(:)) &gt; 0.2862/2))*dl;</code>
<code>h=line(Filter(:,1), ShiftedFilter(:)*60, 'Color','green');</code>
<code>drawnow;</code>
<code>%evaluating snr using power</code>

FilteredCorona = ShiftedFilter(:) .* Corona(:,2);
FilteredSolar = ShiftedFilter(:) .* (Solar(:,2)/175);
snr = sum(FilteredCorona) / sum(FilteredSolar);
snr_no_filterin=sum(Corona(:,2)) / sum(Solar(:,2)/175);
if (snr > snrMax)
snrMax = snr;
BestFilter(1) = n*dl + Corona(1,1);
BestFilter(2) = FilterWidth;
BestFilter(3) = snrMax;
BestFilter
end
if (snr_no_filterin > snr_no_filterinMax)
snr_no_filterinMax = snr_no_filterin;
Best(1) = n*dl + Corona(1,1);
Best(2) = FilterWidth;
Best(3) = snr_no_filterin;
Best
End
%displaying original filter with bw=0.3nm
if (width == 1.771)
BestFilterOld(1) = n*dl + Corona(1,1);
BestFilterOld(2) = FilterWidth;
BestFilterOld(3) = snr;

BestFilterOld
end
if (h ~=0)
%removes line
delete(h);
end
end
end
end
%interpolate wavelengths so that the wavelengths are in equal steps
function NewSpectrum = ConvertFilters(OldSpectrum)
OldLamda = OldSpectrum(:,1);
OldIntensity = OldSpectrum(:,2);
MinLamda = OldLamda(1);
MaxLamda = OldLamda(length(OldLamda));
Range = MaxLamda - MinLamda;
LamdaStep = Range / length(OldLamda);

NewSpectrum = zeros(length(OldLamda), 2);
n = 1;
for lamda = MinLamda:LamdaStep:MaxLamda-LamdaStep
lamda
Intensity = interpolate(OldSpectrum, lamda);
NewSpectrum(n,1) = lamda;
NewSpectrum(n,2) = Intensity;
n = n+1;
end
end
function Intensity = interpolate(OldSpectrum, lamda)
NumEntries = length(OldSpectrum(:,1));
for i=[1:NumEntries-1]
lamda1 = OldSpectrum(i, 1); lamda2 = OldSpectrum(i+1, 1);
intensity1 = OldSpectrum(i, 2); intensity2 = OldSpectrum(i+1, 2);
if (lamda1 <= lamda) && (lamda2 > lamda)
if (lamda1 == lamda)
Intensity = intensity1;
break;
else
m = (intensity2 - intensity1) / (lamda2 - lamda1); % linear interpolation
c = (intensity2 - m * lamda2);

Intensity = m * lamda + c; % y = mx + c
break;
end
end
end
end
end
%evaluating transmission at specific wavelength
function Tx=FilterTx(lamda, Filter)
dl=(Filter(length(Filter(:,1)))-Filter(1,1)) / length(Filter(:,1));
N = (lamda-Filter(1,1))/dl + 1;
N1=floor(N);
N2=N1+1;
if (N2 <= length(Filter(:,1)))
T1=Filter(N1,2);
T2=Filter(N2,2);
Tx = (N-N1)*(T2-T1)/(N2-N1) + T1;
else
Tx = 0;
end
end
%resample original filter in steps determined by dl2
function NewFilter = resample(x, Filter)
dl=(Filter(length(Filter(:,1)))-Filter(1,1)) / length(Filter(:,1));

<code>dl2=dl*x;</code>
<code>NewFilter=zeros(length(Filter(:,1)), 1);</code>
<code>%wavelength determined by sample number and dl2</code>
<code>for s=[1:length(Filter(:,1))]</code>
<code>    LastWavelength = Filter(length(Filter(:,1)),1);</code>
<code>    lamda=(s-1)*dl2+Filter(1,1);</code>
<code>    if (lamda &lt;LastWavelength)</code>
<code>        %transmission determined using wavelength calculated</code>
<code>        Tx=FilterTx(lamda, Filter);</code>
<code>        NewFilter(s,1)=Tx;</code>
<code>    end</code>
<code>end</code>
<code>end</code>
<code>function PlotAll(Corona, Solar)</code>
<code>    figure('Name', 'Spectra', 'Position', [1, 550, 600, 400]);</code>
<code>    title('NewFilter')</code>
<code>    xlabel('Wavelength (nm)')</code>
<code>    line(Corona(:,1),Corona(:,2),'Color','blue');</code>
<code>    ax1 = gca;</code>
<code>    set(ax1,'XColor','red','YColor','blue');</code>

<code>%set(ax1,'XLim',[378 440]);</code>
<code>set(ax1,'YLim',[0 0.04]);</code>
<code>set(ax1,'XGrid','on','YGrid','on')</code>
<code>legend('Corona',2);</code>
<code>ylabel('Irradiance (uW/cm^2/nm)');</code>
<code>ax2 = axes('Position',get(ax1,'Position'), 'YAxisLocation','right', 'Color','none', 'XColor','white','YColor','red');</code>
<code>set(ax2,'YLim',[0 1]);</code>
<code>line(Solar(:,1),Solar(:,2)/175,'Color','red','Parent',ax2);</code>
<code>ylabel('Irradiance (uW/cm^2/nm)')</code>
<code>legend('Solar',1);</code>
<code>end</code>